TEKTONIKA

Kinematics and Dynamics of Multi-stage Salt Diapirs in the Dutch-Central Graben, Southern North Sea

Gerardo Gaitan *[1], **Adam Jürgen** [1]

[1]Department of Earth Sciences, Royal Holloway University of London, Egham, UK

Abstract **Salt structures are of significant economic and societal interest for the energy industry, forming hydrocarbon traps and serving as potential sites for energy storage. The thorough evaluation of multi-stage salt structures and the salt-encasing sedimentary sequences is paramount to mitigate risks and uncertainties in subsurface exploration. Utilizing a recently published methodology applied to a Two-Way-Travel-Time 3D seismic reflection dataset, time-structural, and isochron maps, this tectonostratigraphic study validates regional findings in a local context within the Dutch-Central Graben, Southern North Sea. This study subdivides the Dutch-Central Graben into five structural domains, analyzes the relationship between seismic stratigraphic sequences and sedimentary thickness variations, and provides a deeper understanding of salt diapirism. The study reveals that approximately 53% of salt diapirs in the Dutch-Central Graben were triggered as salt anticlines in the main central graben domain and in the east margin and shoulder domains. Additionally, 36% were triggered as reactive diapirs across the Dutch-Central Graben and 11% as passive diapirs in the west shoulder, east margin, and main rift graben domain. The tallest salt diapirs displayed up to five local stages of salt diapirism across three regional phases of tectonic evolution: rift, contraction/inversion, and post-tectonic. Further, the study evinces that fault communication between nearby salt structures is more common during the salt anticline stage in the rift phase of tectonic evolution in the Southern North Sea, and that radial faults are not characteristic of a particular diapiric stage. These results enhance the understanding of the spatio-temporal variability of salt diapirs on a local scale, the development and evolution of salt-related radial and concentric faulting and provide a useful framework for analyzing salt structures at different scales.**

Executive Editor:
G. Peron-Pinvidic
Associate Editor:
L. Muniz-Pichel
Technical Editor:
Mohamed Gouiza

Reviewers:
Mar Moragas
Anonymous

Submitted:
19 January 2024
Accepted:
21 November 2024
Published:
19 January 2025

1 Introduction

An innovative classification for multi-stage salt structures by *Gaitan and Adam* (2023) demonstrated the potential to characterize the regional variability of salt structures through time and space; nevertheless, this regional study did not address salt-related faulting within the seismic stratigraphic sequences. This study aims to investigate the applicability of the published methodology for salt structures on a local scale, using a 3D seismic dataset of the Dutch-Central Graben sub-basin of the Southern North Sea to analyze thickness variations and elucidate the fault behavior within the seismic stratigraphic sequences encasing salt structures (Figure 1).

The Dutch-Central Graben is an ideal laboratory for studying multi-stage salt structures as salt structures evolved through three regional tectonic phases of the SNS and up to five diverse local stages of salt diapirism (*Gaitan and Adam*, 2023). Salt diapirs respond differently to regional and local deformation processes (*Harding and Huuse*, 2015; *Hudec and Jackson*, 2007; *Hudec et al.*, 2009; *Hudec and Jackson*, 2009; *Jackson et al.*, 1994; *Pichel and Jackson*, 2020; *Vendeville and Jackson*, 1992a,b, 1990). Complex salt diapirs in the Dutch-Central Graben developed due to a basement-inherited rift-graben morphology of the SNS, leading to syn-depositional thickness variations of the Late Permian Zechstein salt (*Peryt et al.*, 2010). Incidentally, a paleo-depositional salt thickness in the Dutch-Central Graben has been documented to be around 500-1,000 m thick (*Maystrenko et al.*, 2012, 2013; *Veen et al.*, 2012).

Understanding the complete evolution of salt structures is paramount to the energy sector, specifically for alternative energy sources (*Duffy et al.*, 2023). Unsurprisingly, there is a renewed interest to study salt structures in the SNS for CCUS, geothermal, and energy storage projects (*Doornenbal et al.*, 2019). Consequently, this study applies a published regional methodology to classify salt structures in a local

*✉ Gerardo.Gaitan@spglobal.com

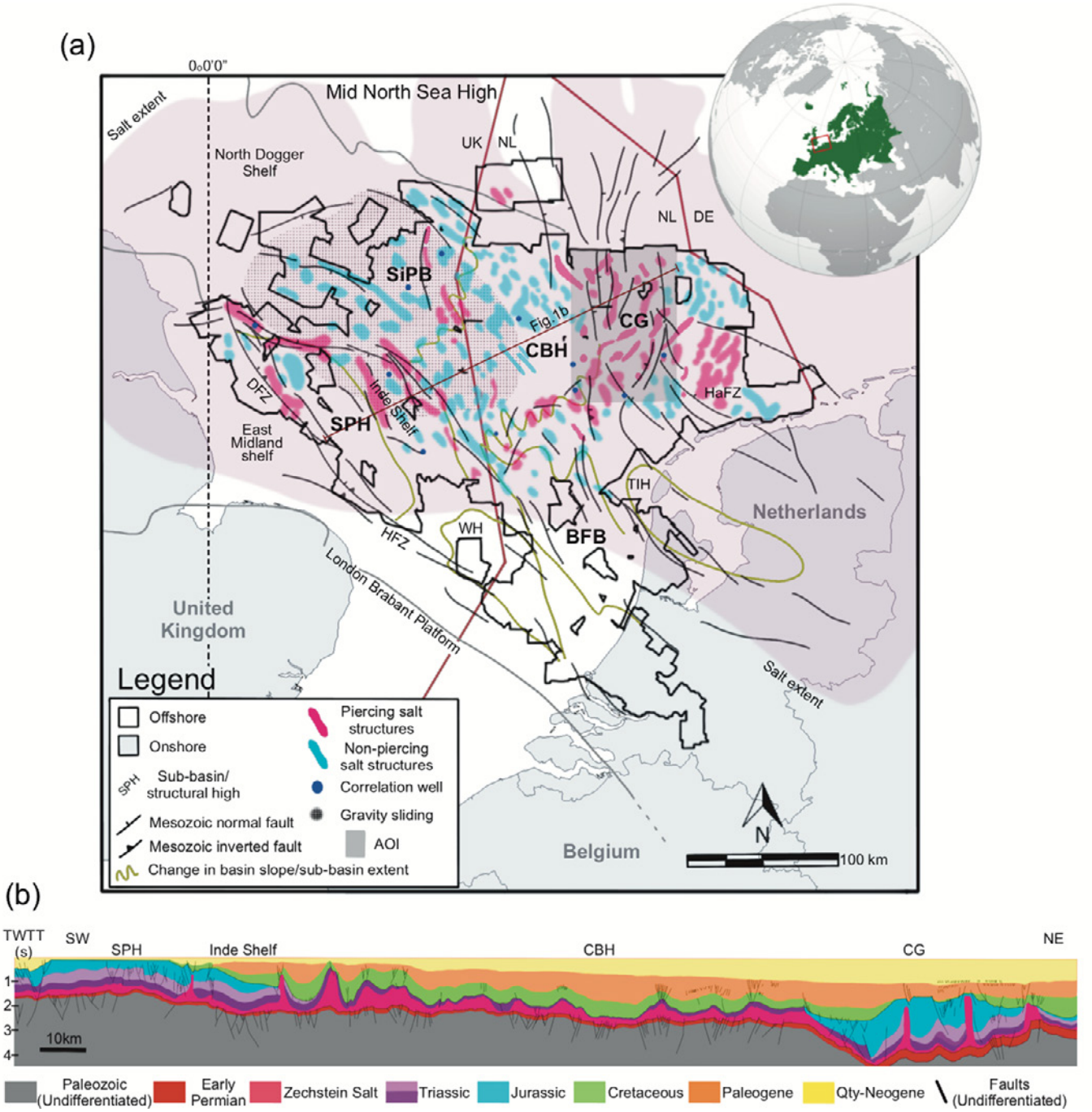

Figure 1 – Regional salt tectonics map of the Southern North Sea salt basin **(a)** and regional cross-section **(b)** of the Southern North Sea passing through the study area after *Gaitan and Adam* (2023). Study area – Central Graben (CG) highlighted by the gray semi-opaque polygon. The Central Graben and study area lies within the Cleaver Bank High (CBH) and the Hantum Fault Zone (HaFZ) in the Dutch part of the Southern North Sea. b) Regional NW-SE cross-section of the Southern North Sea, from the Sole Pit High (SPH), through the Cleaver Bank High, to the west of the Central Graben after *Gaitan and Adam* (2023). BFB=Broad Fourteens Basin, DFZ=Dowsing Fault Zone, HFZ=Hewett Fault Zone, SiPB=Silver Pit Basin, TIH= Texel Ijselmeer High, WH=Winterton High.

context and further characterizes salt-related faults encasing salt structures. Incorporating salt-related fault information into the methodology provides a detailed understanding of the salt structural evolution and deformation processes within the Dutch-Central Graben. Faults associated with salt structures, i.e., radial and concentric faults, offer insights into the stages of diapiric growth, salt mobilization, and diapiric collapse (Figure 2) (*Davison et al.*, 2000; *Jackson and Hudec*, 2017; *Nikolinakou et al.*, 2014; *Stewart*, 2006, 2007) . By including fault information, the methodology better captures the dynamic interactions between salt structures and surrounding stratigraphic sequences, leading to a more accurate and comprehensive characterization of the basin's tectonic history. In the SNS, fault communication and concentric faults have been documented during the Cretaceous, whereas radial faults are more prominent during the Cenozoic (*Harding and Huuse*, 2015). Fault characterization is

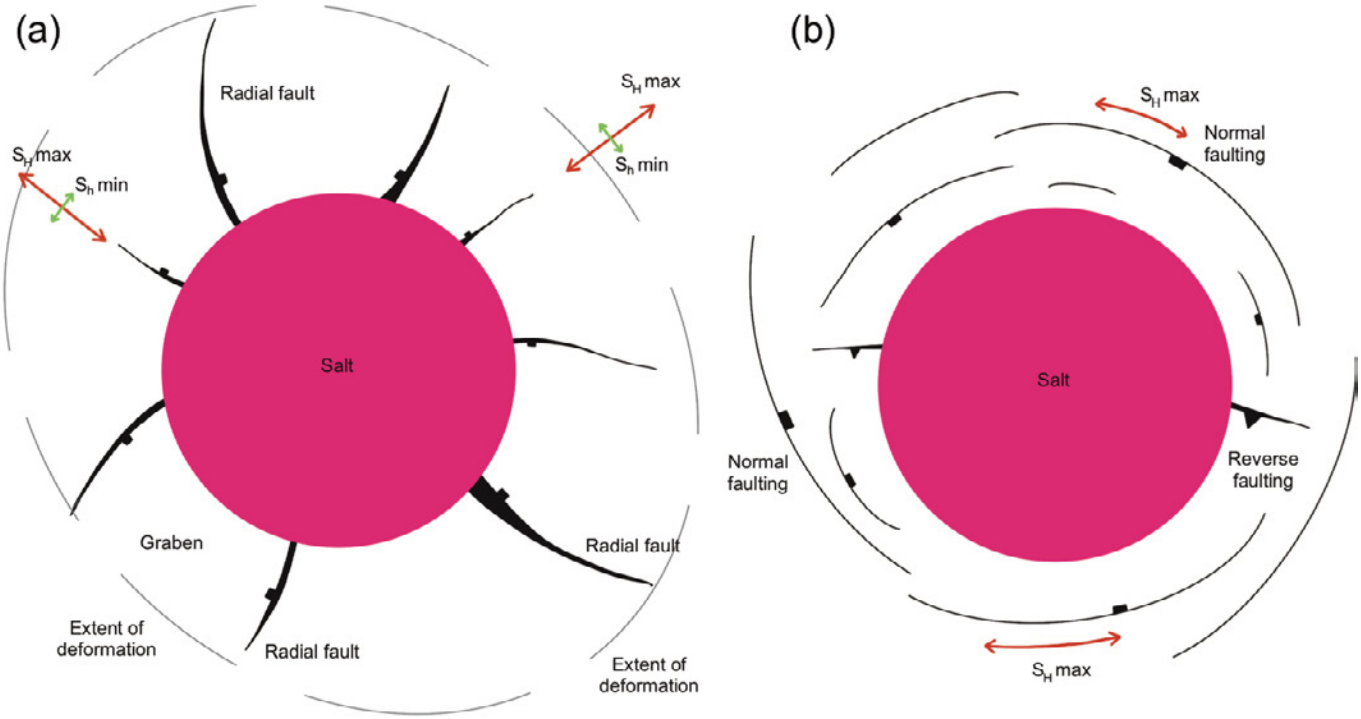

Figure 2 – Cartoon representation of radial **(a)** and concentric **(b)** faults.

valuable to the energy sector because understanding fault behavior aids to the interpretation of reservoir compartmentalization and hydrocarbon migration pathway analysis.

This study utilizes regional seismic stratigraphic sequences, and seismic-derived and geometrical seismic attribute maps to characterize near-diapir thickness variations across the different structural domains of the Dutch-Central Graben and salt-kinematic indicators. Additionally, this study classifies all salt structures in the Dutch-Central Graben and unravels the complete kinematic and dynamic evolution of salt structures from the base of the Late Permian Zechstein salt to the Seabed.

2 Geology of the Central Graben

The study area is in the Central Graben (CG) within the SNS salt basin (Figure 1). The SNS is a post-Variscan, intra-continental salt basin which developed on mid-Paleozoic crustal units of a crystalline Caledonian-Variscan basement platform (*Guterch et al.*, 2010). The Central Graben is a regional failed rift system, characterized by Late Triassic-Jurassic horst and graben structures (*Evans et al.*, 2003).

The Dutch-Central Graben forms part of a larger CG system which extends beyond the Mid North Sea High, from offshore the Netherlands to Norway (Figure 1a). The Dutch-Central Graben in the study area is a complex regional Mesozoic rift graben, trending NW-SE to N-S, where Mesozoic normal faults dip toward the center of the CG system (*Doornenbal and Stevenson*, 2010; *Geluk*, 2005; *Sears et al.*, 1993; *Ziegler*, 1990). The Dutch-Central Graben is bounded to the east by the Hantum Fault Zone, a WNW-ESE trending strike-slip system which extends into onshore the Netherlands (*de Jager and Geluk*, 2007). To the south, the CG is bounded by the Texel Ijselmeer High, and to the west, by the Cleaver Bank High (*Quirk*, 1993). The Dutch-Central Graben system is characterized by a rift graben with a thick Mesozoic-Cenozoic syn-rift and post-rift basin fill (Figure 1b). Pulses of regional rifting during the Mesozoic controlled the sedimentation and preservation of over 1,000 meters of syn-rift sediments and paleo-depocenters in the Dutch-Central Graben (*Jackson and Stewart*, 2017). Subsequently, tectonic rifting triggered salt tectonics and salt diapirism across the different structural domains of the Dutch-Central Graben (*de Jager*, 2003; *Remmelts*, 1996; *Veen et al.*, 2012). Sustained rifting and sedimentation in the Dutch-Central Graben controlled the evolution of salt structures across the Dutch-Central Graben. Pulses of Alpine tectonic contraction during the Late Cretaceous-Cenozoic promoted the thick-skinned inversion of structural elements (*Cameron et al.*, 1992; *Gaitan and Adam*, 2023; *Pharaoh et al.*, 2010). During the Alpine orogeny, the supra-salt Mesozoic cover experienced shortening and contraction of salt diapirs, salt thrusting, uplifting of salt-diapir-flanking seismic stratigraphic sequences, and widespread erosion of uplifted sediments.

2.1 Tectonostratigraphy of the Central Graben

The seismic stratigraphic succession of the Dutch-Central Graben includes several mega-sequences; it is comprised of pre-rift clastics and the Zechstein salt layer, the syn-rift stratigraphic sequence, which represents the transition from shallow marine to open marine conditions, post-rift or syn-contraction marine regressive and transgressive sequences, and the post-tectonic shallow marine clastics (Figure 3) (*Doornenbal and Stevenson*, 2010; *Peryt et al.*, 2010; *Pharaoh et al.*, 2010; *Stewart and Coward*, 1995).

2.1.1 Pre-rift

The Dutch-Central Graben formed during the development of the SNS as a response to the post-Variscan collapse and extensional subsidence during the Permian (*Cameron et al.*, 1992). Pre-rift sequences were deposited during pulses of sea-level rise and periodic flooding which promoted the repeated evaporation and sedimentation of carbonates and evaporites of the Late Permian Zechstein Supergroup (*Jackson and Stewart*, 2017; *Peryt et al.*, 2010). The Late Permian Zechstein salt was deposited in a sabkha environment over aeolian Lower Permian Rotliegend sandstones (*Gast et al.*, 2010; *Glennie and Provan*, 1990). According to *Maystrenko et al.* (2013), in the Dutch-Central Graben, paleo-salt thickness reached c. 500 to 1,000 m, whereas in northern Germany, the Zechstein salt reached over 1,500 m of thickness (*Pharaoh et al.*, 2010).

Pre-rift carboniferous coal measures are the principal gas source in the SNS. The Lower Permian Rotliegend sandstones are an important hydrocarbon reservoir, effectively sealed by the Late Permian Zechstein salt layer (*Stewart and Coward*, 1995).

2.1.2 Syn-rift

The syn-rift stratigraphic sequences in the Dutch-Central Graben were controlled by regional thermal relaxation of the lithosphere which promoted the change from marine conditions into continental/deltaic conditions during the Early Triassic (Figure 3) (*Ziegler*, 1990). Lower Triassic sediments accumulated gradually and over a generally flat area in the Dutch-Central Graben. However, small Lower Triassic thickness variations across the Dutch-Central Graben have been documented and attributed to Early Triassic halokinesis in the CG in the Central North Sea (*Hodgson et al.*, 1992) and in the Dutch-Central Graben (*Gaitan and Adam*, 2023).

The Triassic Hardegsen and Early Cimmerian pulses of rifting controlled shallow marine incursions which led to the development of intra-Middle to Late Triassic evaporitic intervals, e.g., the Röt and Muschelkalk halite members (*Pharaoh et al.*, 2010). The North Sea rift system remained active during the Early Jurassic in the Dutch-Central Graben which marked the transition of the SNS from shallow marine to fully and open marine conditions, promoting the lithostratigraphic change from sandstones to marly and fined-grained sediments (*Cameron et al.*, 1992).

2.1.3 Post-rift and/or Syn-contraction/Inversion

The Cretaceous post-rift and syn-contraction/inversion stratigraphic sequence is characterized by the transition from a shallow marine environment to open and deep marine conditions (*Vejbæk et al.*, 2010). Further, it is characterized by the deposition of argillaceous marly sediments and the formation of reefal limestones during the sub-Hercynian pulses of inversion as a response to the Alpine collision from continental Europe. Locally within the Dutch-Central Graben, the transition from the syn- to post-rift phases is characterized by thick and tabular Early Cretaceous sediments which were later uplifted and eroded due to tectonic inversion. The sub-Hercynian orogeny was the first of numerous pulses of contraction during the Late Cretaceous-Cenozoic in the SNS (Figure 3) (*Coward and Stewart*, 1995; *Stewart and Coward*, 1995).

2.1.4 Post-tectonic

The post-tectonic stratigraphic sequence in the Dutch-Central Graben is characterized by Oligocene-Neogene shallow marine, fine-to-coarse grained clastics deposited during a phase of tectonic quiescence and a basin-wide eastward basin tilt due to the thermal relaxation from the Alpine orogeny (*Grant et al.*, 2019).

2.2 Salt Tectonics in the Central Graben

Density differences within the thick Zechstein salt layer represent diverse stratigraphic lithologies, e.g., carbonates, anhydrite, halite, and clastics, which triggered the syn-depositional deformation of the Zechstein layer (*Jackson and Stewart*, 2017). An early structurization of the Zechstein salt layer promoted the syn-deposition of Lower Triassic sediments, triggering halokinesis which led to the formation of salt anticlines and salt pillows (*Clark et al.*, 1998; *Gaitan and Adam*, 2023; *Jackson and Stewart*, 2017).

During the Triassic-Jurassic, rifting of the continental crust promoted halokinesis and salt diapirism in the Dutch-Central Graben (*Remmelts*, 1995). Salt flow into the Dutch-Central Graben basin and coeval thick sedimentation, controlled the sustained evolution of salt diapirs in the basin center (*Veen et al.*, 2012); consequently, the tallest salt structures in the SNS are found in the Dutch-Central Graben (*Gaitan and Adam*, 2023).

Pulses of contraction during the late Mesozoic-Cenozoic inverted parts of the

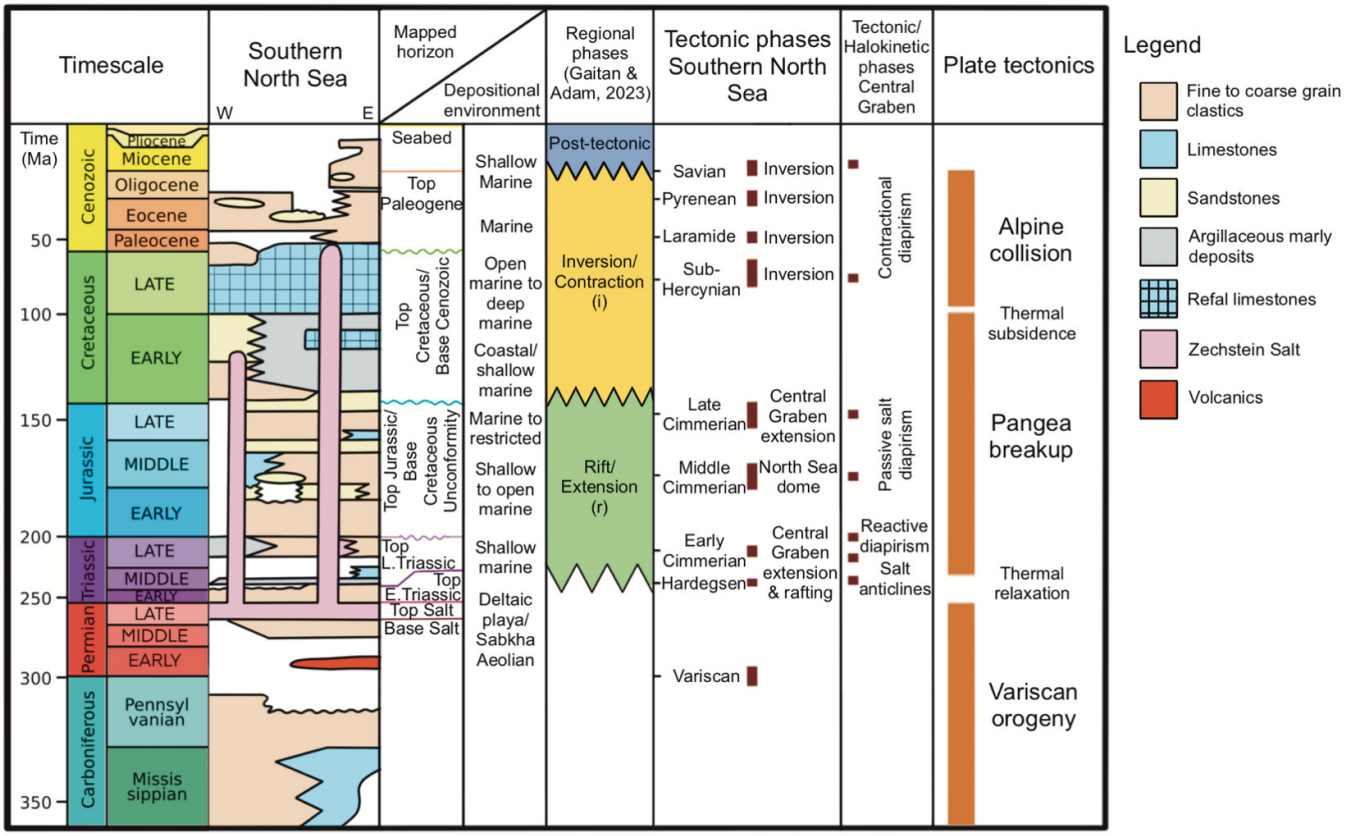

Figure 3 – Simplified lithostratigaphic succession of the Southern North Sea basin and regional phases with emphasis in the Central Graben after *Gaitan and Adam* (2023).

Dutch-Central Graben and reactivated salt diapirs (*Glennie*, 1998). The salt kinematics and salt-related deformation of individual salt diapirs in the North Sea have been documented by *Stewart* (2007) in the Central and Southern North Sea and by *Harding and Huuse* (2015) in the Hantum Fault Zone, Dutch-SNS. Further, *Gaitan and Adam* (2023) documented that multi-stage salt diapirs in the Dutch-Central Graben commenced as salt anticlines, evolving through two regional phases and up to five local stages of salt diapirism.

3 Dataset and Workflow

3.1 Dataset

We used the regional SNS MegaSurvey 3D full stack seismic reflection dataset, originally provided by Petroleum Geo-Services (PGS), for the analysis of the kinematics and dynamic processes of salt diapirs in the Dutch-Central Graben. The SNS MegaSurvey consists of forty-four 3D time-migrated seismic volumes. Survey merging of the SNS MegaSurvey was performed for the post-stack time migrated volumes using post-stack techniques. The horizontal inline and crossline spacing of the seismic dataset is 50 m and the vertical sample rate is 4 ms.

The study area is the Dutch-Central Graben in the SNS and is 6,970 km^2 large (Figure 1a). Seismic picks of six regional seismic horizons were provided by PGS in the original seismic dataset (Figure 4): 1) base Zechstein salt, 2) top Zechstein salt, 3) top Early Triassic, 4) top Triassic, 5) Base Cretaceous Unconformity (BCU), and 6) top Cretaceous (Base Cenozoic). Two further regional seismic horizons, i.e., the top Paleogene (Base Neogene) and Seabed, were interpreted and mapped across the study area for a total of eight survey-wide horizons (Figure 4). The overall quality of the MegaSurvey 3D seismic dataset in the Mesozoic-Cenozoic succession is good. Imaging problems related to the high P-wave velocities of salt are expected, for instance, velocity pull-ups beneath salt structures, seismic noise, multiples near the steep flanks of salt diapirs, and vessel-acquisition trace problems in the first 300-600 ms Two-Way-Travel-Time (TWTT) from the seabed.

3.2 Workflow

This study utilized the methodology and nomenclature proposed in *Gaitan and Adam* (2023) for the identification, mapping, and classification of salt structures in the Dutch-Central Graben. Moreover, we highlight the evolution of seven salt structures across the study area, which were identified to be the most complex and some of the tallest salt structures across the SNS. The methodology consists of, 1) the piercing and structural relationship analysis of salt structures using TWTT structural maps, 2) time-thickness variation analysis, 3) characterization

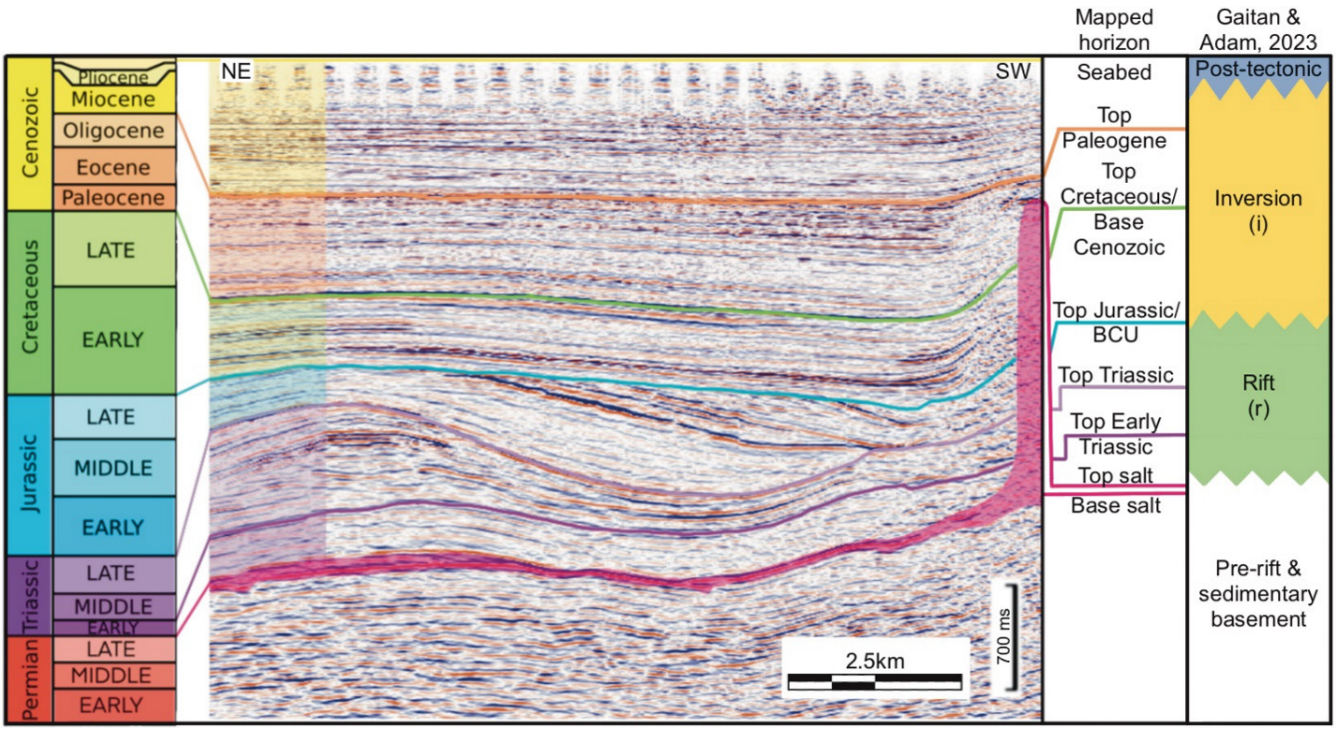

Figure 4 – Seismic stratigraphy of the Dutch-Central Graben. Mapped seismic stratigraphic horizons used for this study and their relationship with the regional phases of the Southern North Sea after *Gaitan and Adam* (2023). Seismic data courtesy of PGS (now TGS).

of salt-withdrawal paleo-depocenters in the different structural domains of the study area using time-thickness maps to discriminate active salt structures from inactive salt structures, and 4) the analysis of near-diapir, second order structural elements using seismic TWTT attribute maps to highlight salt diapirism, salt collapse processes, and near-field stress behavior of salt structures during their evolution.

This study systematically correlated all salt structures across the different structural domains of the Dutch-Central Graben. First, we utilized the regionally mappable seismic horizons and tectonostratigraphic sequences and linked them to the regional phases in *Gaitan and Adam* (2023), e.g., pre-kinematic, detached, rift, inversion/contraction, and post-tectonic phases (Table 1). We utilized the regional phases because they link the basin-scale tectonic processes and the tectonostratigraphic sequences across the different structural domains of the Dutch-Central Graben. The local stages are linked to the regional phases. Using the local stages, we identified and compared all salt structures across the study area. For instance, using the local stages, we studied the different processes controlling the evolution of salt structures, e.g., differential loading, sedimentation, erosion, and gravitational processes. Consequently, we linked the local processes which further control salt diapirism to the regional phases by analyzing time-thickness variations within the seismic stratigraphic sequences, unraveling different stages of salt mobilization.

We created a total of eight TWTT structural maps using the regional seismic stratigraphic horizons shown in Figure 4. The TWTT structure maps in stratigraphic order are: 1) base Zechstein salt, 2) top Zechstein salt, 3) top Early Triassic, 4) top Triassic, 5) top Jurassic/Base Cretaceous Unconformity (BCU), 6) top Cretaceous/base Cenozoic, 7) top Paleogene/base Neogene, 8) top Quaternary-Neogene/Seabed. The TWTT structure maps highlight the location, geometry, distribution, and piercing relationships of salt structures. For example, salt anticlines and salt pillows are positive-relief structural features in structure maps, whereas salt diapirs are also represented by positive-relief structures but salt diapirs pierce the overlying structure maps, leaving a gap in younger structure maps.

Time-thickness maps, i.e., isochrons, were computed between two interpreted horizons, or structure maps, to reflect the local thickness variations around salt structures. We generated a total of seven isochron maps: these are, 1) top Zechstein salt-base Zechstein salt, 2) top Early Triassic-top Zechstein salt, 3) top Late Triassic-top Early Triassic, 4) BCU-top Late Triassic (for thickness variations in the Jurassic stratigraphic sequence), 5) top Cenozoic-BCU, 6) top Paleogene-top Cenozoic, and 7) Seabed-top Paleogene. We assumed that during salt mobilization, salt-withdrawal paleo-depocenters, i.e., depositional thicks, form next to salt structures as salt mobilization creates space where salt is being withdrawn from the salt source to feed salt structural growth. Accordingly, salt diapirism renders depositional

Table 1 – Nomenclature for classification of multi-stage salt structures after *Gaitan and Adam* (2023). *Pre-kinematic and Detached phases not discussed in this study.

Regional Phase	Regional ID	Diapiric sequence	Concordance	Phase	Driving mechanisms	Kinematic Stage	Local Stage
Post-tectonic	pt	Diapiric	Discordant	Piercing	Halokinetic	Passive diapir	dP
		Post-diapiric	Concordant	Non-piercing	Inactive	Dormant diapir	dD
		Pre-diapiric	Concordant	Non-piercing	Inactive	Salt anticline/pillow	pA
					Halokinetic		
Incversion/ Contraction	i	Diapiric	Discordant	Piercing	Halokinetic	Passive diapir	dP
				Arrested	Tectonically Active	Contractional diapir	dC
						Salt thrust	dT
		Pre-diapiric	Concordant	Non-piercing	Tect. active	Contractional anticline	pC
					Halokinetic	Salt anticline	pA
Rift	r	Diapiric	Discorant	Piercing	Halokinetic	Passive diapir	dP
					Tect. active	Extension	dE
				Arrested	Tect. active	Reactive diapir	dR
		Pre-diapiric	Concorant	Non-piercing	Halokinetic	Salt anticline/pillow	pA
Detached *	d	Diapiric	Discorant	Piercing	Halokinetic	Passive diapir	dP
				Arrested	Tectonically Active	Active diapir	dA
						Reactive diapir	dR
		Pre-diapiric	Concorant	Non-piercing	Tect. active	Salt anticline/pillow	pA
Pre-kinematic *	pk	Diapiric	Discorant	Piercing	Halokinetic	Passive diapir	dP
		Pre-diapiric	Concorant	Non-piercing		Salt anticline/pillow	pA
		Layered	Concorant	-	Inactive	Layered	iL
			Regional identifiers		Local identifiers		

thicks which are highlighted using isochron maps. By analyzing depositional thicks and comparing different isochron maps, we unravel the evolution of salt structures. Additionally, we interpreted seismic stratigraphic thins which may develop atop pre-diapiric and arrested salt structures. We acknowledge that stratigraphic thins also form due to drape sedimentary compaction and other depositional processes not discussed in this study.

A similarity attribute volume was computed on the seismic dataset and similarity maps were extracted from the mapped TWTT structure maps. Similarity attribute maps permitted an identification of faults by enhancing lateral changes in impedance contrast. We utilized similarity maps for the analysis and interpretation of structural features from the different structural domains of the study area and from the different salt structural domains of salt diapirs, e.g., salt's flanks, body, and carapace. Second order structural features are ubiquitous to all salt basins and help understanding the complete kinematic and dynamic evolution of salt structures. For example, radial faults form around active salt diapirs, whereas the absence of radial faulting infers passive diapirism or inactive stages (Figure 2a). Contrarily, concentric faulting indicates stages in which salt structures deflate or collapse to feed salt diapiric growth on adjacent salt structures (Figure 2b); these kinematic indicators are then linked to the local and regional phases to compare them across all salt diapirs in the study area.

4 Results

4.1 Basement Architecture of the Dutch-Central Graben

The structural configuration of the Dutch-Central Graben is observed using TWTT structure maps from the base Zechstein salt TWTT structural map (Figure 5a), the base Zechstein salt similarity attribute map (Figure 5b), and from regional seismic cross-section profiles of the Dutch-Central Graben (Figures 6-7). The basement architecture of the study area is characterized by NNW-SSE trending regional faults; these series of faults link to form the sub-salt CG system which run from the northwestern to the southern part of the study area. The base Zechstein salt horizon is widely affected by sub-Zechstein salt basement faults across the study area. For instance, the CG margins display areas where secondary faults developed synthetically and antithetically to the marginal faults.

The study area is divided into five structural domains, i.e., the western shoulder, western margin, eastern shoulder, eastern margin, and the main rift graben, i.e., the main CG system. The main rift graben represents the deepest structural levels of the study area; the base Zechstein salt horizon is 4.4 s deep. Further, the structural shoulders

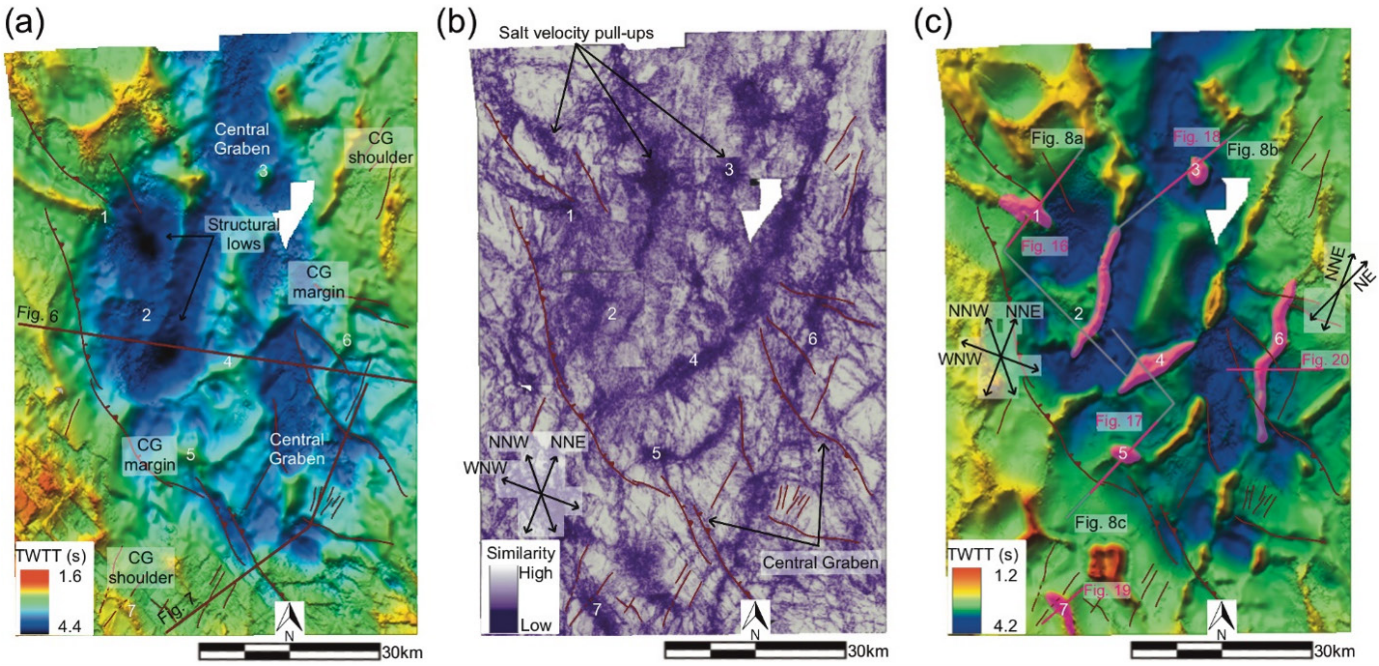

Figure 5 – Zechstein TWTT maps of the Dutch-Central Graben (CG). Salt diapirs 1-7 labeled and highlighted. **a)** Base Zechstein salt structure map with location of regional seismic sections for Figures 6 and 7 shown. CG structural domains' outline shown. At this level, the positive relief structures where salt diapirs are located represent salt velocity pull-ups. **b)** Base Zechstein salt structure map with similarity attribute map applied. Interpreted main and secondary faults shown. Velocity pull-ups associated with overlying salt diapirism also shown. **c)** Top Zechstein salt structure map. Location of Figures 8a-c and 16-20 shown.

represent the structural highs in the study area. Because of the proximity of the western shoulder to the Cleaver Bank High, the western shoulder shares part of the tectonostratigraphy of the Cleaver Bank High. Structural margins, i.e., the western and eastern margins, represent the transition between the structural shoulders and the main rift basin (Figure 5a).

4.2 Salt Structural Relationships

Seismic cross-sections evince the different styles of coupling between sub- and supra-salt faults. For instance, basement-involved, hard-linked coupling is observed at the basin margins of the Dutch-Central Graben and basement-detached deformation is evident in the main rift graben (Figures 6-7). Further, direct coupling between sub-Zechstein salt faults and supra-Zechstein salt faults is evident in the southern part of the Dutch-Central Graben (Figure 7), contrarily, basement-detached deformation is ubiquitous atop salt structures (Figures 6-8).

The salt structural trend in the rift graben ranges from WNW to ENE whereas in the structural margins ranges from N to NNE (Figures 5c and 9a). Moreover, the general salt structural trend interpreted in the western shoulder is NW to NNW, whereas in the eastern shoulder is N to NNE (Figure 9a).

Using the range of the velocities cited in *Geldart and Sheriff* (2004) for average sedimentary sequences (sandstones) encasing salt structures, with ϕ = 20-30% and the starting velocities V0 for Lower Triassic sediments in the Southern Permian Basin (3,590 m/s) (*Schnabel et al.*, 2021) (Schnabel et al., 2021), the height's mean of all salt diapirs identified in the study area is 2,772 m (Figure 9b). The maximum height of the tallest salt diapirs is approximately 4,128 m and the smallest is 1,130 m. We qualitatively defined the tallest salt diapirs as the salt diapirs which are taller than the height's mean of all salt diapirs in the study area, i.e., taller than 2,772 m. The tallest salt diapirs are in the western shoulder, main rift graben, and eastern margin (Figure 9b). In the study area, half of the total interpreted salt diapirs are taller than 2,772 m.

4.3 Structural Domains of the Dutch-Central Graben

4.3.1 Central Graben Shoulders and Margins

The main rift graben is bounded by the structural margins which transition to the structural shoulders to the southeast and northwest (Figures 5a, 6-7). The main basement-inherited structural faults of the rift basin act as the main boundaries between the structural shoulders and margins where deformation is characterized by half-grabens and smaller horst-graben structures (Figures 6-7). The structural shoulders and margins display a general NNW-SSE structural trend orientation in the south and central part of the study area which transition into a N-S structural trend toward the northern part of the study area (Figure 5a).

The western shoulder and margin are

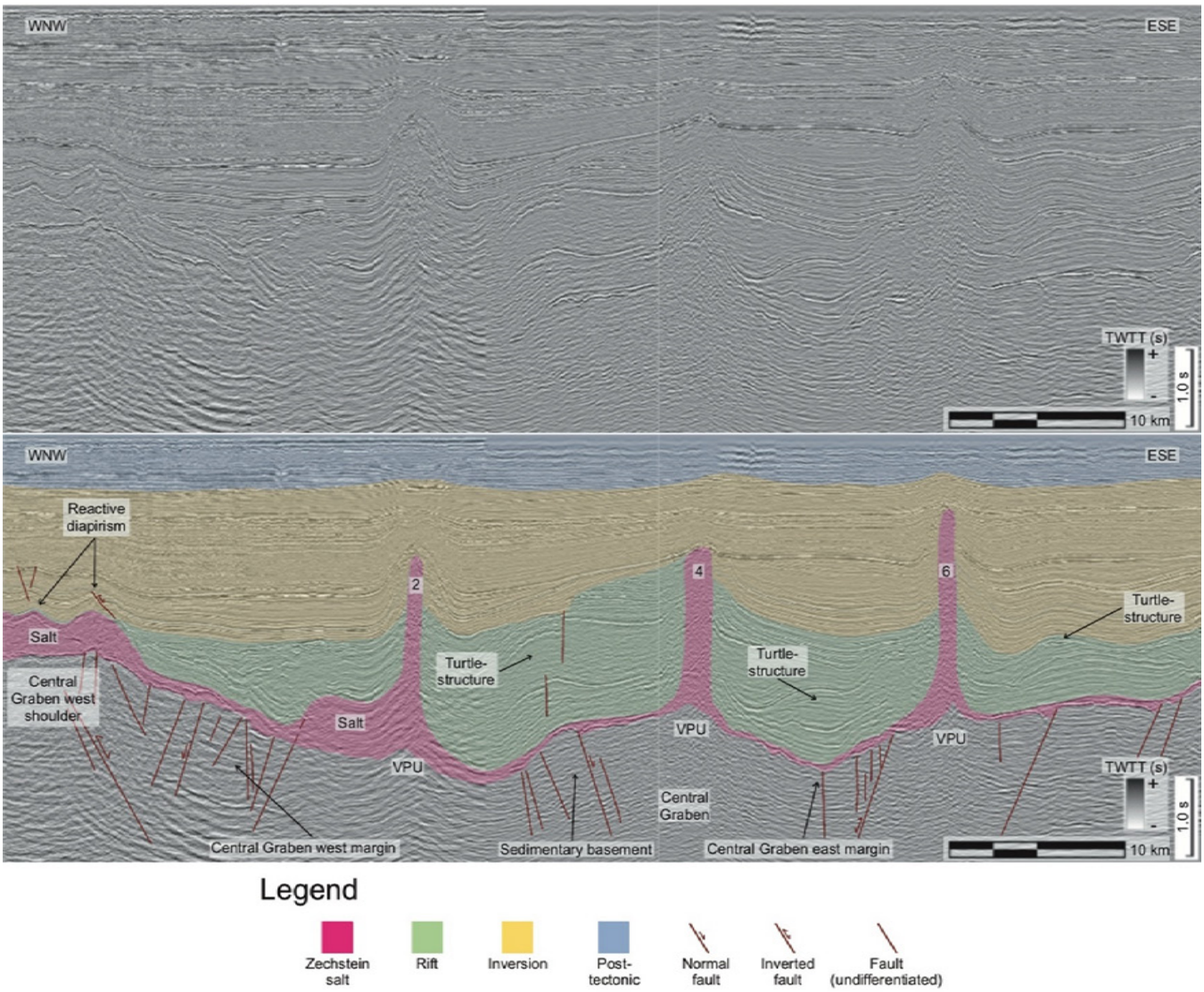

Figure 6 – Regional WNW-ESE seismic section of the Central Graben (CG). Regional seismic-cross section profile cuts obliquely through three salt diapirs, two in the main central part of the CG system (labeled as 2 and 4), and one in the eastern CG shoulder of the study area. Location of cross-section shown in 5a. Seismic data courtesy of PGS (now TGS).

characterized by northeast-dipping normal faults and secondary antithetic faults to the main rift margin faults. The offset values of the main northeast-dipping faults are negligible due to pulses of inversion during the Cretaceous-Cenozoic. Further, the eastern shoulder and margin are characterized by a southwest-dipping normal faults with normal fault throw offsets of c. 0.60 s (Figure 7). The transition from the structural shoulders into the rift graben varies. For instance, there is a drop of c. 1.0 s over 13 km from the structural shoulder to the rift graben in the central-western part of the study area (Figure 6). Moreover, there is a gentler drop of c. 0.6 s over 15 km from the structural shoulder into the main rift graben in the southwestern part of the study area.

4.3.2 Central Graben System

The main rift graben is characterized by a general N-S structural trend (Figure 5a, c) and is bounded by the NNW-SSE trending structural shoulders.

The structural configuration of the main rift graben is characterized by structural highs and lows, i.e., grabens controlled by basement-related faulting and inversion at the sedimentary-basement level (Figure 6). Regional seismic cross-sections through the main Dutch-Central Graben show a typical pre-rift salt basin in which the salt layer thickness varies gradually across the Dutch-Central Graben rather than abruptly varying across the horst and graben basement structures (Figure 7).

4.4 Seismic Stratigraphy and Regional Phases

We used the regional phases from *Gaitan and Adam* (2023) for the systematic identification, mapping, and classification of salt diapirs in the Dutch-Central Graben, because the regional phases are derived from the regional tectonic phases and the observed seismic stratigraphic characteristics of the SNS (Table 1). Incidentally, this study does not discuss the pre-kinematic and detached regional phases as they

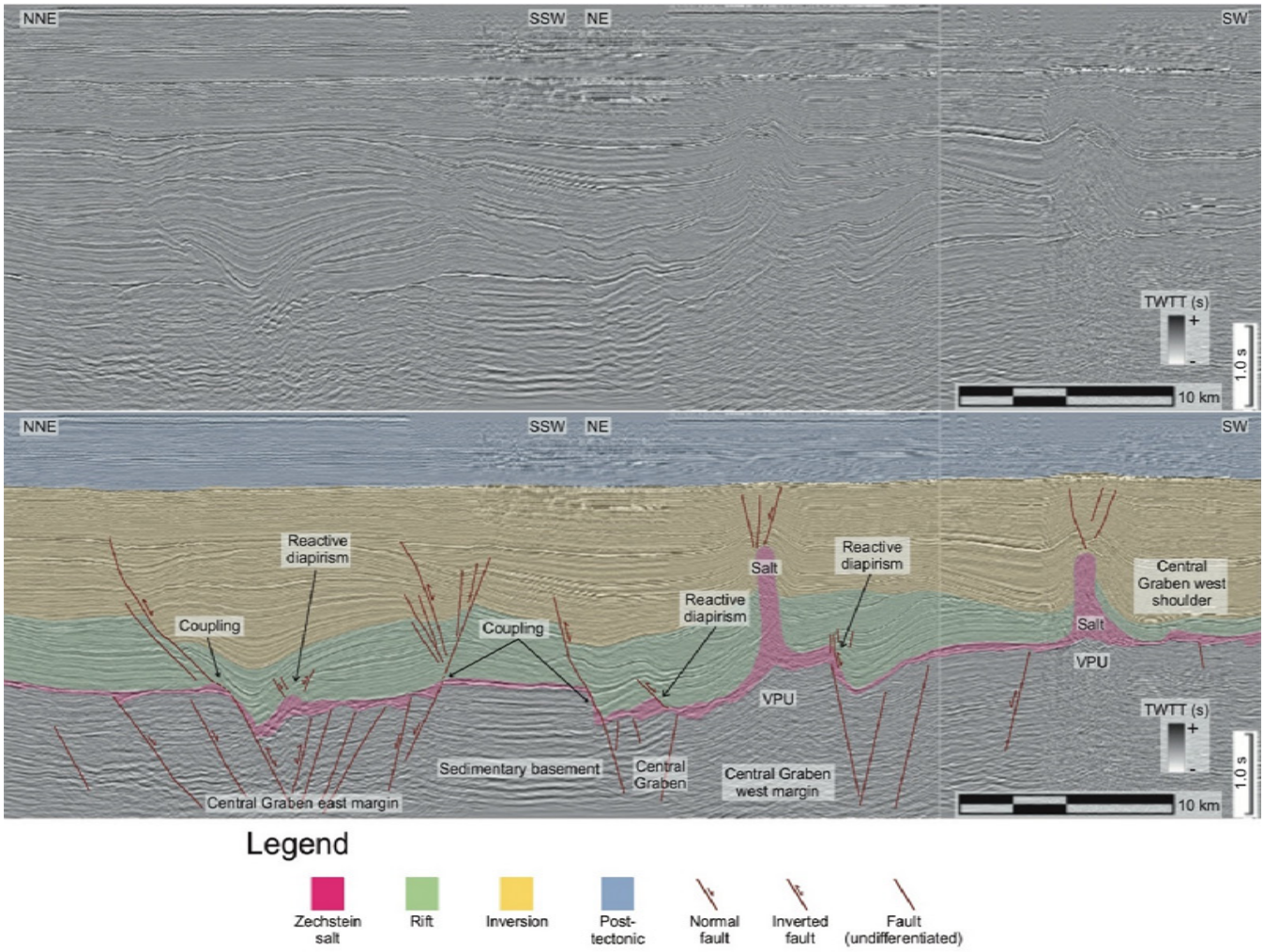

Figure 7 – Arbitrary-regional, NNE-SSW to NE-SW trending, seismic section of the Central Graben (CG). Regional seismic-cross section profile cuts perpendicular to the main CG system and cuts obliquely through two salt diapirs, one in the western margin of the CG and the remaining one in the shoulder section of the study area which belongs to the Cleaver Bank High. Location of cross-section shown in 5a. Seismic data courtesy of PGS (now TGS).

are irrelevant for the Dutch-Central Graben.

4.4.1 Rift Regional Phase

The rift regional phase is composed of three seismic stratigraphic sequences, i.e., Early Triassic, Mid-Late Triassic, and Jurassic (Figure 4). The top Early Triassic is a lithological unconformity boundary and displays high amplitudes; it represents the downward transition from argillaceous marly deposits and evaporites to siliciclastics (Figures 3-4). Additionally, it is characterized by a semi-continuous, medium-amplitude reflectors. The top Triassic boundary is also a lithological boundary and represents the downward transition from clastics to marly deposits; it is represented by a medium-amplitude reflector which top-laps the crests and flanks of salt diapirs and is truncated by salt diapirs piercing the top Triassic seismic stratigraphic boundary (Figure 6). Lastly, the BCU stratigraphic boundary is a basin-wide unconformity, semi-continuous, mid- to high-amplitude reflector.

Broadly, the seismic characteristics of the rift regional phase are complex and vary across the study area, e.g., in the northern part of the study area, the rift stratigraphic sequence drapes over the east-dipping western Central Graben fault forming a structural monocline (Figure 8a). Moreover, the seismic reflector characteristics range from chaotic to reflection-free which indicate a convoluted deformation of the stratigraphic sequences in the rift phase. Syn-halokinetic stratigraphic sequences adjacent to salt diapirs display discontinuous to subparallel seismic reflectors, which evince salt diapirism processes in the rift phase (Figure 8). During the rift regional phase, inverted salt-withdrawal basins are ubiquitous across the Dutch-Central Graben which educe a widespread halokinetic stage.

Seismic stratigraphic sequence thicknesses in the rift regional phase varies across the different structural domains of the Dutch-Central Graben. For instance, the seismic stratigraphic sequence developed during the rift regional phase, is thicker in the northern part of the study area (Figure 8b) and within the Dutch-Central Graben system (Figure 8c). Reactive diapirism and syn-kinematic

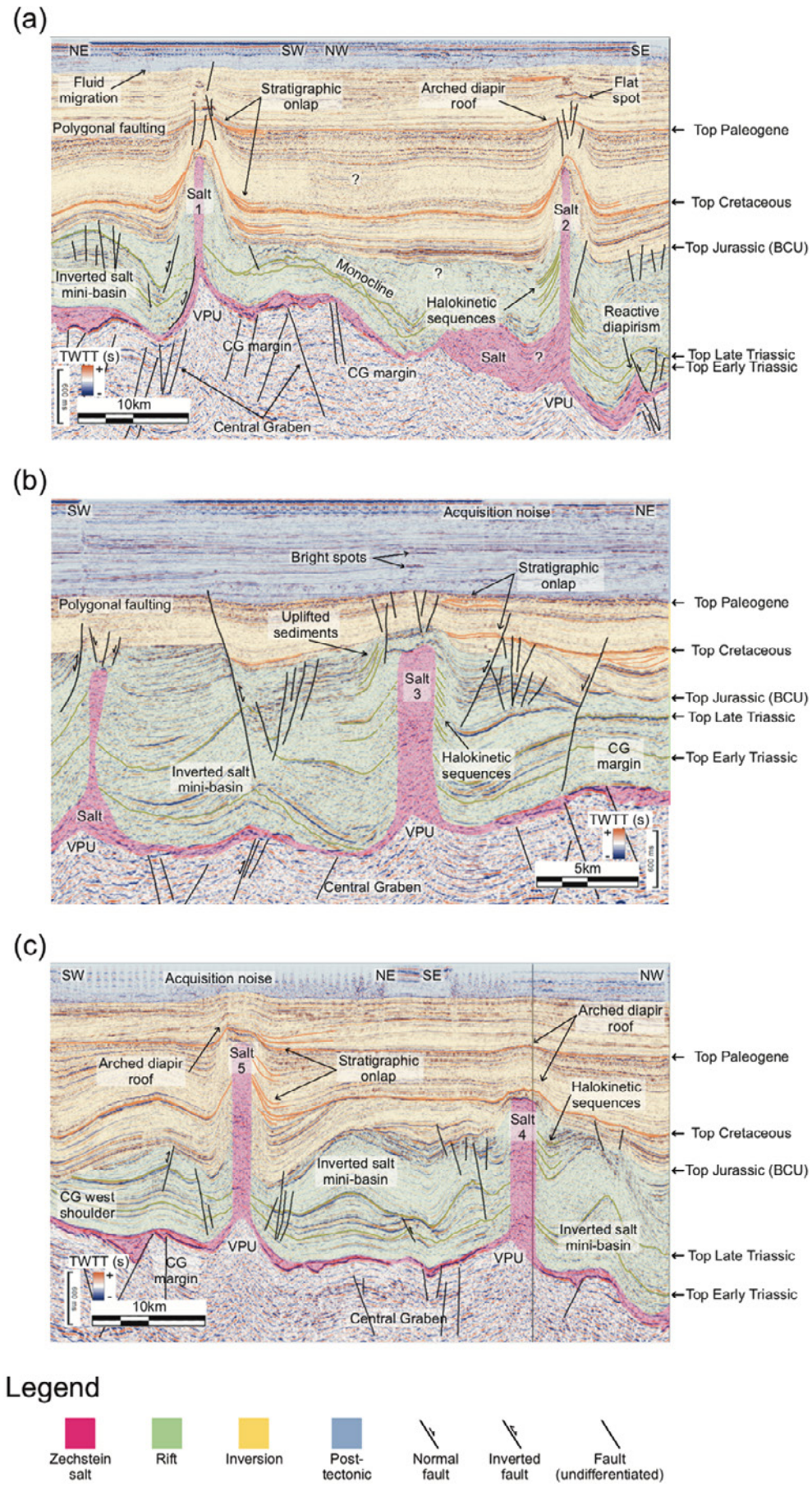

Figure 8 – Interpreted regional seismic sections of the Dutch-Central Graben. Location of seismic cross-sections in Figure 5c.

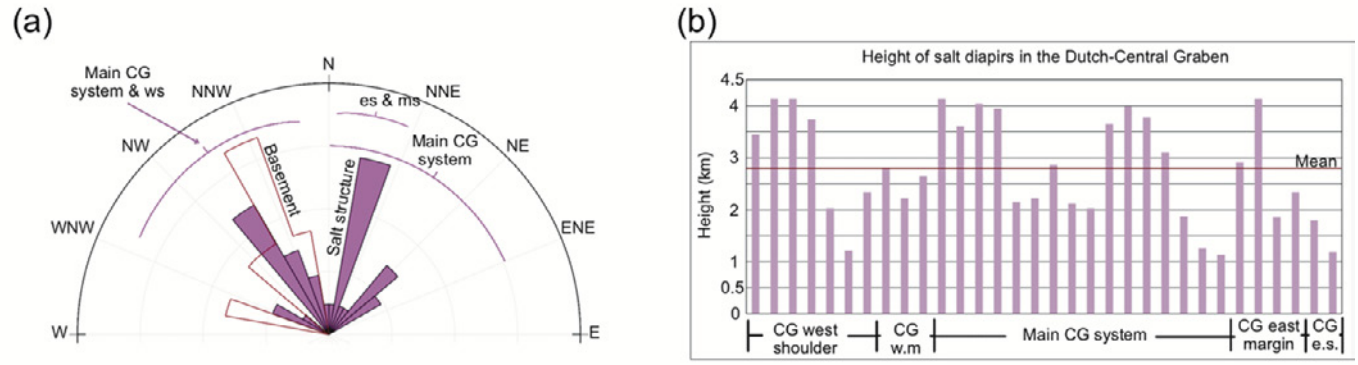

Figure 9 – Analysis of Salt diapirs in the Central Graben (CG). **a)** Rose diagram of the salt structural trend in the CG and structural sub-domains. No secondary fault's trend shown. Ws = west shoulder, es = east shoulder, ms = margins. **b)** Height/thickness of salt diapirs in the CG in kilometers. The mean is = 2,772 m.

sedimentation elucidate a rifting stage in the main Central Graben system and western margin (Figure 8a). Nevertheless, most of the active faults in the rift regional phase developed to accommodate halokinesis and salt diapirism processes. The true geometries of faults and their respective fault-throws are overprinted by inversion at a later stage.

4.4.2 Inversion Regional Phase

The inversion regional phase is composed of two to three seismic stratigraphic sequences, i.e., the Cretaceous, Paleogene, and part of the Neogene stratigraphic sequences (Figure 4). For simplicity and because this study did not map the top Early Cretaceous, the Cretaceous mega-stratigraphic sequence during the inversion phase also includes the post-rift transition from the rift to the inversion regional phase. Generally, the post-rift transition during the Early Cretaceous is recorded as a quiescent period where Lower Cretaceous stratigraphic sequences are tabular and fill structural lows, i.e., Early Cretaceous sediments display stratified, onlaps, and pinch-out stratigraphic geometries (Figures 4 and 8).

The top Paleogene often coincides with the transition from the stratigraphic sequences in the inversion to the post-tectonic regional phase (Figure 8b). The top Cretaceous stratigraphic boundary is a geological conformity displaying a high-amplitude reflector; this boundary represents the downward transition from Cenozoic siliciclastics to Upper Cretaceous reefal limestones (Figures 3-4 and 8a, c). Near salt diapirs, the reefal limestones are absent because of erosional processes linked to salt diapirism and tectonic uplift (Figure 8b). Similarly, the top Paleogene displays high-amplitude seismic characteristics and is unpierced by salt diapirs. At this regional phase, the seismic stratigraphic sequences are thicker to the west (Figure 8a, c) and thinner in northern part of the Dutch-Central Graben (Figure 8b).

During the Cretaceous, subparallel to divergent stratigraphic sequences evidence active faulting and salt diapirism processes. Additionally, Cretaceous stratigraphic reflectors pinch-out toward the crest of salt diapirs (Figure 8a-c). Figure 8 shows that the Paleogene stratigraphic sequence is continuous and tabular, characterized by parallel to subparallel reflectors. The lower stratigraphic layers in the Paleogene display a transparent seismic expression, transitioning into brighter seismic reflectors toward the Paleogene-Neogene stratigraphic boundary; this is attributed to differential compaction during the Paleogene. Generally, the Paleogene stratigraphic sequence is characterized by widespread polygonal faulting, which suggests sedimentary compaction and dewatering processes. In addition, syn-kinematic seismic reflectors and extensional faulting in the Paleogene elucidate salt mobilization and diapirism processes (Figure 8b). The Paleogene stratigraphic sequence is uplifted and faulted at the carapace of salt diapirs which represents late stages of contractional diapirism (Figure 8a, b).

4.4.3 Post-tectonic Regional Phase

The post-tectonic regional phase is represented by the Quaternary-Neogene seismic stratigraphic sequences (Figure 4). Figures 6-8 show that seismic stratigraphic characteristics of the post-tectonic regional phase are characterized by parallel to divergent reflectors. High and low amplitude seismic reflectors during the Quaternary-Neogene represent the transition from fine clastics to interbedded sandstone layers.

The first 300-600 ms TWTT from the seabed are fragmented due to acquisition and seismic related noise, rendering the interpretation of the first stratigraphic seismic reflectors challenging. The post-tectonic regional phase represents the regional phase in which salt structures become dormant, consequently, gentle seismic stratigraphic onlap is common atop older seismic stratigraphic sequences uplifted during the inversion regional phase (Figure 8).

4.5 Early Triassic – Early Rift Phase

The salt structural trend of evolving salt structures across the study area during the Early Triassic varies from NW-SE to NNE-SSW, which is consistent with the structural trend of sub-salt basement structures and Early Triassic faults, i.e., NNW-SSE and NNE-SSW, respectively (Figure 10a).

The Dutch-Central Graben is represented by a N-S trending, regional structural low (Figure 10a). In the main rift basin, the salt structural trend varies from NNE to NE which is consistent with the documented Early Triassic active faults (Figures 9a and 10a). Additionally, NNE-SSW trending, structural highs in the main rift basin are interpreted to represent inverted salt-withdrawal structures, i.e., turtle structures. The main salt structural trend in the eastern shoulder and margin is NNE, which is oblique to the main structural trend of the sub-salt rift system, but consistent with the Early Triassic structural trend (Figures 9a and 10a).

4.5.1 Thickness Variations and Local Paleo-depocenters

Local paleo-depocenters (pds) were interpreted from the Early Triassic isochron map where time-thickness are > 0.42 s; pds during the Early Triassic represent early stages of salt mobilization during the rift regional phase (Figure 10b).

Based on structural trend analyses, we interpret the development of pds on the western margin to be associated with the regional basement fault trend and halokinetic processes (Figure 10b). Consequently, NNE-SSW trending pds during the Early Triassic triggered halokinesis in the eastern shoulder and margin. A higher number of pds in the northern Dutch-Central Graben during the Early Triassic suggests that rifting occurred from north to south (Figure 10b).

4.5.2 Salt Mobilization and Local Stages of Salt Diapirism

The dominant salt structures during the Early Triassic are salt anticlines observed in the western margin, main graben, and eastern shoulder; these are characterized by early salt-withdrawal pds trending oblique to perpendicular to the main structural trend of the sub-salt basement faults (Figure 10). A less dominant salt structure are reactive diapirs observed at the margins of the study area and influenced by marginal extension of sub-salt basement faults and halokinesis in the main rift basin (Figures 7 and 10). Additionally, only one passive diapir was identified in the western shoulder.

Lower Triassic syn-sedimentation developed salt-withdrawal pds (Figure 10c). It is interpreted that deposition of Lower Triassic sediments was influenced by an extant topography and uneven Zechstein salt layer; this is inferred by the NNE-SSW structural axial plane of Early Triassic pds in the main graben.

4.6 Middle and Late Triassic – Rift Phase

The main salt structural trend of salt structures during the Mid-Late Triassic is NE (Figure 11), which is consistent with the NNE-SSW structural trend of active Mid-Late Triassic faults, but oblique to the interpreted NNW-SSE basement structural trend (Figure 11a). Moreover, Mid-Late Triassic sediments are absent in the western and northwestern part of the study area (Figure 11a-b). Similarly, Mid-Late Triassic faults in the western margin display the general NNW-SSE structural trend interpreted during the Early Triassic.

The Dutch-Central Graben is represented by an N-S regional structural low in the central-north part of the main rift basin (Figure 11a-b). Like in the Early Triassic, NNW-SSW trending structural highs in the main rift basin represent salt-withdrawal structures (Figure 11).

4.6.1 Thickness Variations and Local Paleo-depocenters

Local paleo-depocenters (pds) were interpreted from the Mid-Late Triassic map where time-thicknesses > 0.61 s (Figure 11b); pds during the Mid-Late Triassic represent stages of salt mobilization and phases of tectonic rifting.

The development of pds in the southern part of the western margin is interpreted to be controlled by rifting of the NNE-SSW trending faults in the main rift graben and linked to halokinetic processes of NNE-SSW trending salt structures (Figure 11b). Generally, pds switched from the northern part of the main rift graben in the Early Triassic to the central-south part during the Mid-Late Triassic; this is interpreted to be controlled by the subsidence of the main rift basin and active faulting during the Mid-Late Triassic (Figure 11b). Further, local pds within the main rift basin shifted closer to salt structures which represents changes in salt diapiric growth modes.

Structural highs in the center of the main rift graben are interpreted as NNE-SSW, inverted pds elucidated by structural maps and local pds in isochron maps (Figure 11a-b). In the eastern margin, NNE-SSW trending salt diapirism is evinced by the development of pds (Figure 11b).

4.6.2 Salt Mobilization and Local Stages of Salt Diapirism

The dominant salt structures during the Mid-Late Triassic are passive diapirs observed across the study area: evidenced by salt-withdrawal pds which shifted closer to salt diapirs (Figure 11c). Less dominant salt structures are salt anticlines observed only in the main rift basin. Moreover, based on the evolution of pds, we interpreted salt diapir “3” in the northern

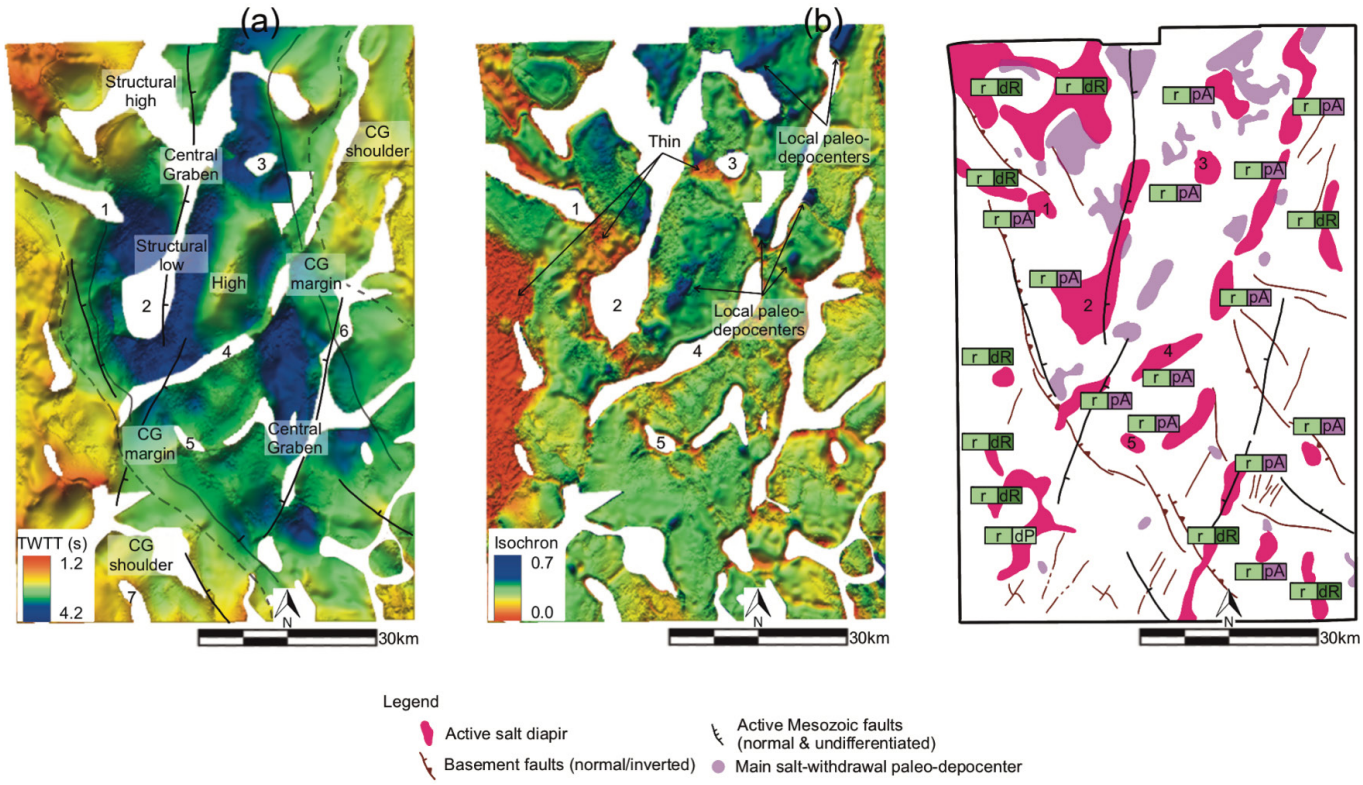

Figure 10 – Early Triassic (rift) seismic stratigraphic level. **a)** TWTT structure map. **b)** Top Early Triassic – Top Zechstein salt TWTT thickness map (isochron). **c)** Synthesis map of the Early Triassic mega-stratigraphic sequence in the rift regional phase showing main salt-withdrawal paleo-depocenters and underlying basement faults. Salt diapirs 1-7 labeled. Gaps represent areas where salt structures have pierced through the stratigraphic horizon in a) and b).

part of the main rift graben to transition from a salt anticline to a passive diapir during the Mid-Late Triassic (Figures 10c and 11c).

Pulses of North Sea rifting during the Late Triassic triggered N-S faults in the northern part of the study area and NNE-SSW to the south (Figure 11). Rifting and basement-involved deformation promoted the accumulation of thick Upper Triassic sediments (Figure 11b-c). Consequently, we interpreted rifting and thick sedimentation to be the main driving mechanisms for the transition of salt anticlines to a passive diapiric stage. This is evidenced by the Mid-Late Triassic pds shifting closer to NNE/NE trending salt structures in the main rift graben, eastern margin, and eastern shoulder.

4.7 Jurassic – Rift Phase

The salt structural trend of evolving salt structures during the Jurassic varies from NNE to NNW, which is oblique to parallel to the NNW-SSW sub-salt basement structural trend, respectively (Figure 9a), but consistent with the N to NNE Jurassic faulting (Figure 12a). Like in the Mid-Late Triassic, the Jurassic stratigraphic sequence is mostly absent in the western and eastern shoulders.

The Dutch-Central Graben is represented by structural highs and lows within the main N-S trending, main rift graben (Figure 12a). Like in the Mid-Late Triassic, the structural highs represent inverted salt-withdrawal structures. Contrarily, structural lows represent stratigraphic sequences adjacent and at the flanks of salt structures.

4.7.1 Thickness Variations and Local Paleo-depocenters

Paleo-depocenters (pds) were interpreted from the Jurassic isochron map where time-thicknesses > 2.60 s (Figure 12b). Sediment thicknesses across the study area are generally consistent, except in the southeastern part which are interpreted to be linked to halokinesis and salt diapirism.

Jurassic sediments in the Dutch-Central Graben are thin in the central-north part of the study area and are thicker to the southeast (Figure 12b). The N-S trending, thin area in the central-north part is interpreted to be an erosional surface due to uplift during a younger inversion regional phase. Generally, pds shifted from the center of the main rift graben during the Mid-Late Triassic to the structural margins during the Jurassic (Figure 12b).

4.7.2 Salt Mobilization and Local Stages of Salt Diapirism

Passive diapirs are the dominant salt structure in the Jurassic observed in the western margin, main Central Graben rift basin, and eastern margin characterized by adjacent salt-withdrawal pds and a general NNE to NE salt structural trend (Figure 12c).

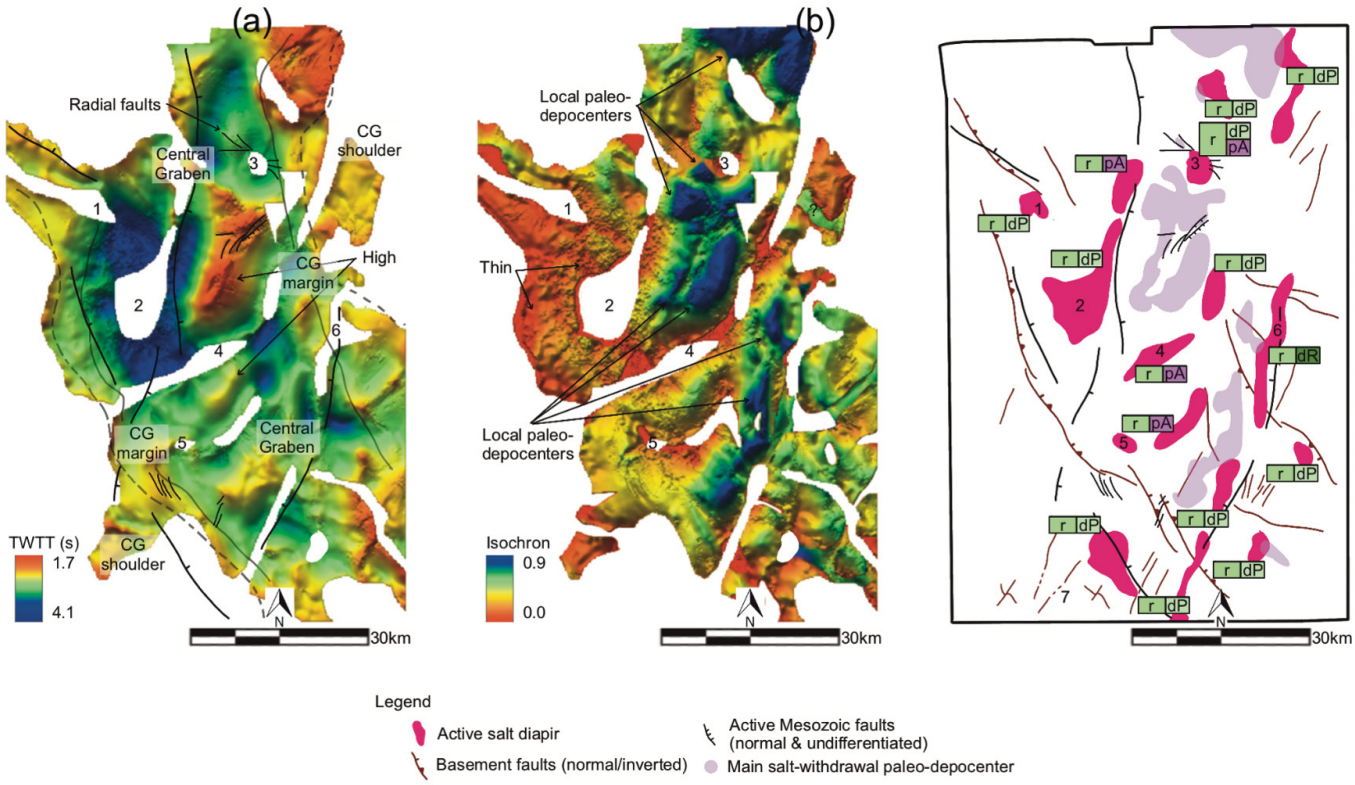

Figure 11 – Mid-Late Triassic (rift) seismic stratigraphic level. **a)** TWTT structure map. **b)** Top Mid-Late Triassic – Top Early Triassic TWTT thickness map (isochron). **c)** Synthesis map of the Mid-Late Triassic mega-stratigraphic sequence in the rift regional phase showing main salt-withdrawal paleo-depocenters, underlying basement faults, and Mesozoic faulting. Salt diapirs 1-7 labeled. Gaps represent areas where salt structures have pierced through the stratigraphic horizon and zones of regional erosion in a) and b). Radial and concentric faulting are observed emanating away from both, salt stocks and salt walls.

The controlling factor for passive diapirism in the Jurassic is the Cimmerian rift tectonic phases of the Southern North Sea which promoted the deposition and preservation of up to 3.0 s of Jurassic sediments in the study area (Figures 8 and 12b). Additionally, pds shifted closer to salt structures from the Mid-Late Triassic to the Jurassic and are interpreted to have recorded the transition from reactive to passive diapirism in the east margin, and from salt anticlines to passive diapirs in the main rift graben (Figures 11c and 12c). Passive diapirs which initiated during the Triassic continued to evolve as passive diapirs during the Jurassic; this is evidenced by the thick sediments surrounding the diapirs in the main rift graben and the absence of salt-related faulting around the salt structures (Figures 7-8).

4.8 Cretaceous – Post-rift and Inversion Phase

The salt structural trend of evolving salt structures during the Cretaceous varies from NNW-SSE to NNE-NE. Salt structures trending NNW-SSE in the western shoulder are consistent with the sub-salt basement structural trend, whereas salt structures trending NNE-NE are consistent with the structural trend of Cretaceous faults (Figure 13a). Further, radial faulting and fault communication are ubiquitous across the study area and suggest active stages of salt diapiric processes during the Cretaceous. For instance, radial faults are present around salt diapir 5 in the main rift graben and at the salt's roof of arrested salt diapir 3 (Figure 13a).

The time-structure map of the Dutch-Central Graben during the Cretaceous is characterized by arrested salt structures trending NW to NE (Figure 13a). Moreover, structural lows adjacent to arrested salt structures are also commonplace, which is interpreted to be the result of salt diapiric processes.

4.8.1 Thickness Variations and Local Paleo-depocenters

Paleo-depocenters (pds) were interpreted from the Cretaceous isochron map where time-thicknesses > 0.82 s (Figure 13b). There is a clear contrast in sediment thickness across the study area during the Cretaceous; sediment thicknesses are thin to the north and thick in the southeast. Thin to absent sediment thicknesses in the north and central part of the main rift graben are interpreted to be an erosional surface due to inversion of the Central Graben during the Late Cretaceous. Contrarily, thick sediments in the eastern part of the study area are interpreted to be the result of erosional redistribution of sediments from adjacent structural highs. Secondarily, salt diapirism also controlled

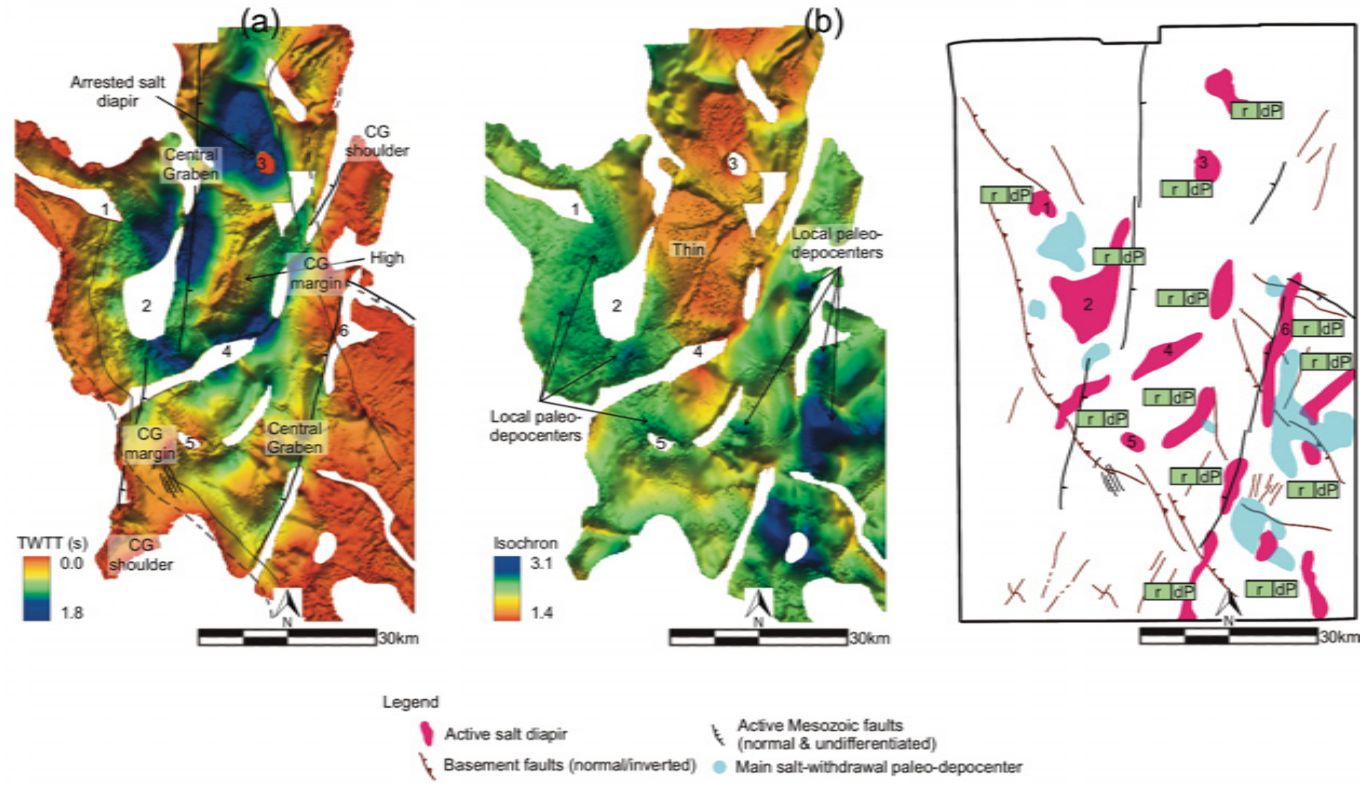

Figure 12 – Jurassic (rift) seismic stratigraphic level. **a)** TWTT structure map. **b)** Top Jurassic (BCU) – Top Mid-Late Triassic TWTT thickness map (isochron). **c)** Synthesis map of the Jurassic mega-stratigraphic sequence in the rift regional phase showing main salt-withdrawal paleo-depocenters, underlying basement faults, and Mesozoic faulting. Salt diapirs 1-6 labeled. Gaps represent areas where salt structures have pierced through the stratigraphic horizon and zones of regional erosion in a) and b).

thickness variations observed in the central rift graben and adjacent to salt structures (Figure 13b).

4.8.2 Salt Mobilization and Local Stages of Salt Diapirism

Contractional salt diapirs are the dominant salt structure in the Cretaceous, controlled by tectonic inversion during the Late Cretaceous (Figure 13). A less dominant salt structure in the Cretaceous is a passive diapir controlled by sedimentary loading observed in the southeastern part of the study area (Figure 13).

The main processes controlling salt diapirism were: 1) thick and sustained sedimentation due to tectonic quiescence during the Early Cretaceous which bolstered the long-lived evolution of passive diapirs during the Cretaceous (Figures 6-8), 2) tectonic inversion which promoted the rejuvenation of salt diapirs across the study area and the change in salt diapiric growth from passive to contractional diapirism (Figure 13c); this is evidenced by uplifted stratigraphic reflectors at the flanks of salt diapirs (Figure 8), positive-relief salt structures in structure maps, and radial faults around salt diapirs (Figure 13a), 3) sediment redistribution from eroded structural highs which controlled the development of pds in the southern part of the study area and promoted passive diapirism (Figure 13b-c).

4.9 Paleogene – Inversion and Contraction Phase

The salt structural trend of evolving salt structures across the study area during the Paleogene varies from NW-SE to NE-SW (Figure 14). NW-SE trending salt diapirs in the western shoulder are consistent with the sub-salt basement structural trend (Figure 5).

Broadly, the Dutch-Central Graben is represented by a structural low to the north and a structural high to the south (Figure 14a); this is interpreted to be the consequence of a regional basin-wide tilt north of the study area during the Neogene. Concentric and normal faulting evince salt structural collapse and salt deflation processes in the western shoulder.

4.9.1 Thickness Variations and Local Paleo-depocenters

Paleo-depocenters (pds) were interpreted from the Paleogene isochron map where time-thickness > 0.84 s (Figure 14b). Regional pds are interpreted to be the result of erosional processes from structural highs in the central part of the study area, which redistributed eroded Late Mesozoic-Paleogene sediments into adjacent pds (Figure 14b). Further, localized pds adjacent to arrested salt structures across the study area are interpreted to be the result of salt diapiric processes.

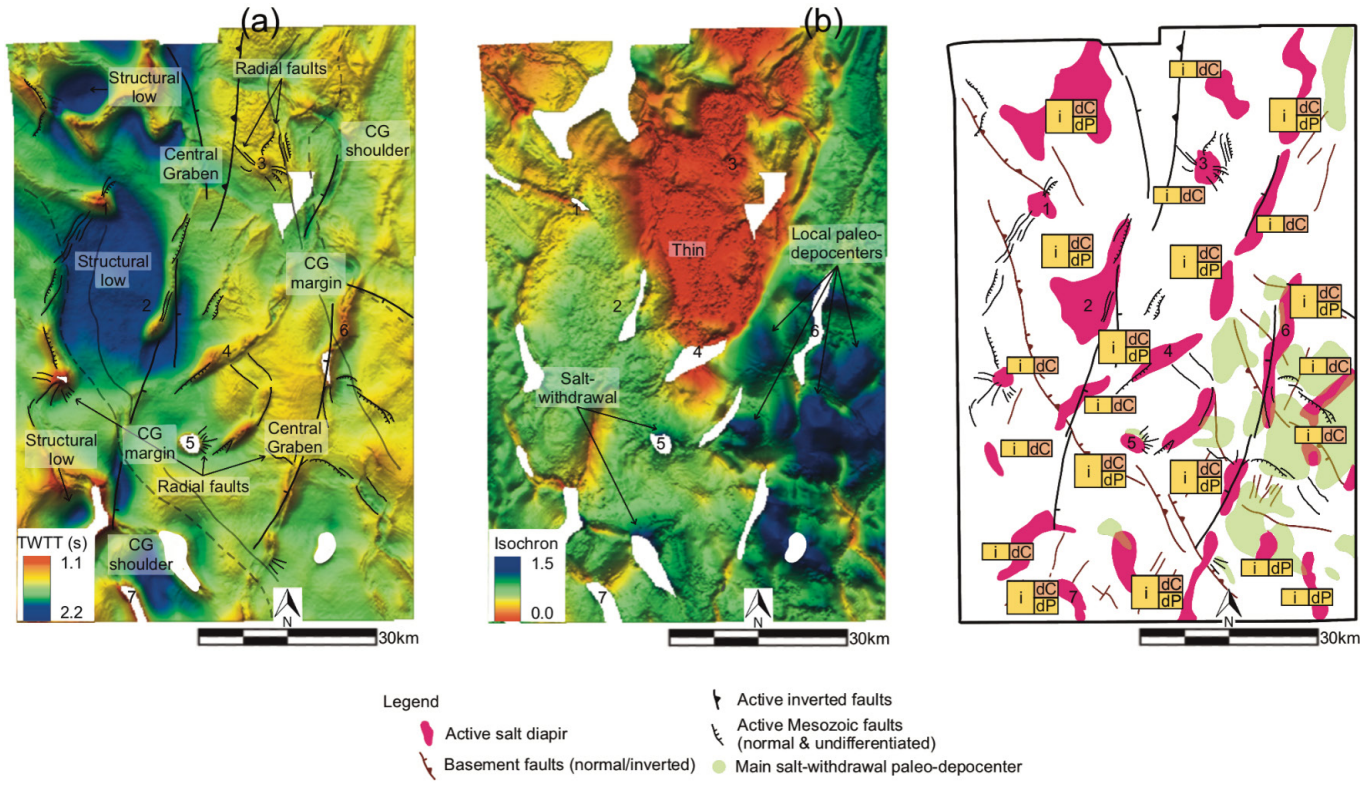

Figure 13 – Cretaceous (inversion) seismic stratigraphic level. **a)** TWTT structure map. **b)** Top Cretaceous (Base Cenozoic) – BCU TWTT thickness map (isochron). **c)** Synthesis map of the Cretaceous mega-stratigraphic sequence in the inversion regional phase showing main salt-withdrawal paleo-depocenters, underlying basement faults, and Mesozoic faulting. Salt diapirs 1-7 labeled. Gaps represent areas where salt structures have pierced through the stratigraphic horizon in a) and b). Radial and concentric faulting are observed emanating away from both, salt stocks and salt walls. Fault communication is observed between salt diapirs.

4.9.2 Salt Mobilization and Local Stages of Salt Diapirism

The dominant salt structures during the Paleogene are contractional salt diapirs across the study area (Figure 14c). We interpreted tectonic shortening to be the controlling factor for contractional salt diapirism during the Paleogene due to the Laramide orogeny, evidenced by positive-relief salt structures (Figure 14a), thin sediments atop salt structures (Figure 14b), and uplifted seismic stratigraphic sequences around squeezed salt diapirs (Figure 8). Accordingly, tectonic shortening is interpreted to continue from the inversion phase which began in the Late Cretaceous, resulting in the long-lasting evolution of salt diapirs during the Paleogene.

4.10 Quaternary-Neogene – Inversion/Contraction and Post-tectonic Phase

Time-structure maps for the Quaternary-Neogene stratigraphic horizon are not shown in this study due to vessel-acquisition trace problems in the first 300-400 ms from the seabed.

Paleo-depocenters (pds) were interpreted from the Quaternary-Neogene isochron map where time-thicknesses > 1.0 s. The Dutch-Central Graben is characterized by regional and local pds in the northern part of the study area (Figure 15).

During the Quaternary-Neogene, all salt diapirs are contractional diapirs and display local thickness variations and thin sediments at the carapace of the salt diapirs during the inversion phase (Figure 15b). Further, all contractional diapirs in the Quaternary-Neogene stratigraphic sequence become dormant as evidenced by parallel and tabular seismic stratigraphic reflectors in the post-tectonic phase (Figures 7-8).

The main process which controlled salt diapirism during the Quaternary-Neogene was remnants of the Alpine collision (Figure 3). Tectonic contraction was still active though the Neogene evidenced by local radial and normal faults interpreted to be due to salt diapirism and salt diapiric collapse, but during the post-tectonic phase, the basin-wide tilt toward the north of the study area further controlled sedimentation and the development of pds observed in isochron maps (Figure 15b).

4.11 Non-tectonic Deformation of Multi-stage Salt Diapirs

The non-tectonic trigger mechanisms of salt diapirs are characterized by syn-sedimentary and syn-halokinetic processes observed across all structural domains of the study area. Non-tectonic

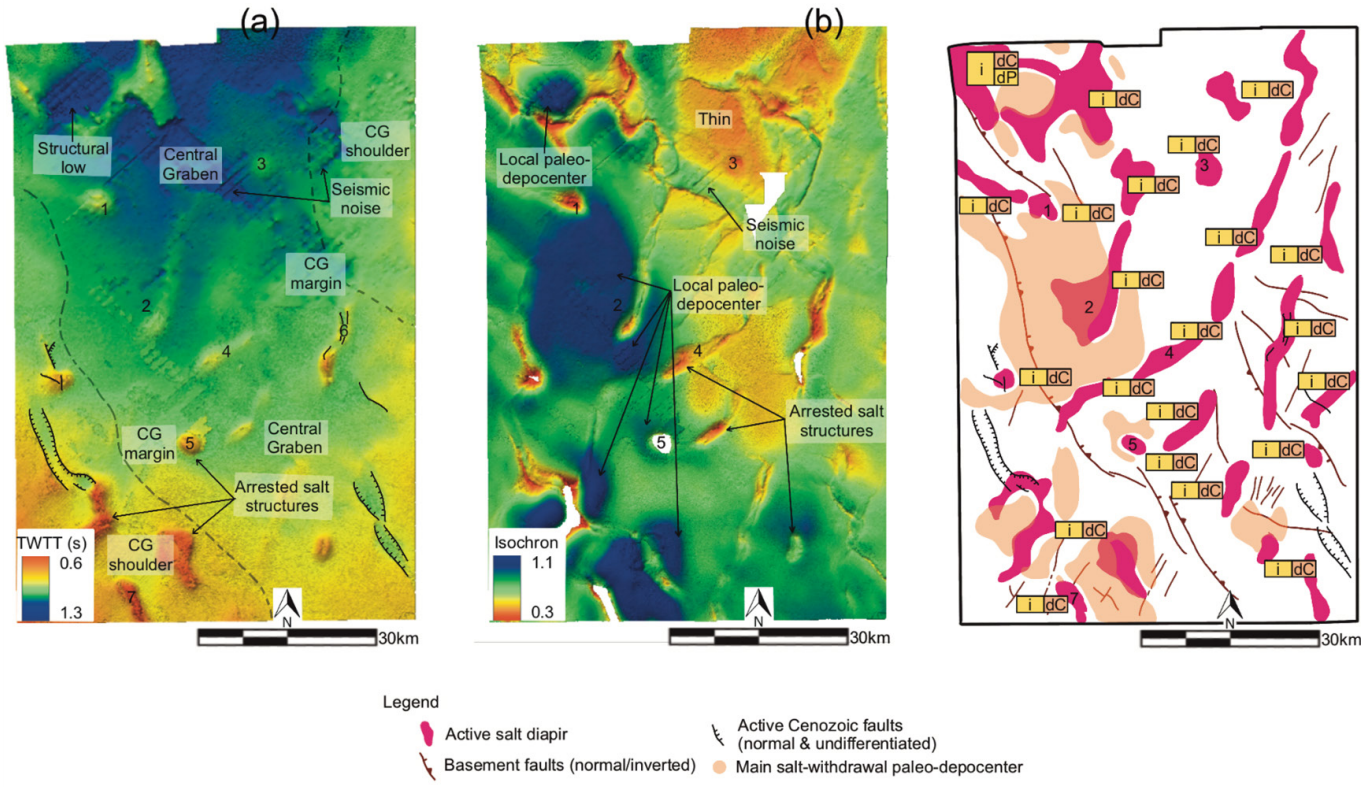

Figure 14 – Paleogene (inversion/contraction) seismic stratigraphic level. **a)** TWTT structure map. **b)** Top Paleogene – Base Cenozoic (Top Cretaceous) TWTT thickness map (isochron). **c)** Synthesis map of the Paleogene mega-stratigraphic sequence in the inversion regional phase showing main salt-withdrawal paleo-depocenters, underlying basement faults, and Cenozoic faulting. Salt diapirs 1-7 labeled. Gaps in b) represent areas where salt structures are arrested within the Paleogene seismic stratigraphic sequence. Mainly concentric faulting is observed atop elongated salt walls.

deformation in the eastern margin is characterized by tabular and pinching-out geometries at the pedestal of multi-stage salt diapir 1, which elucidates early halokinetic processes (Figure 16). Diachronous sedimentation is evidence for early halokinetic rise during the salt anticline stage (Figures 16-17). The absence of salt-related faulting during the salt anticline stage in the Early Triassic and the perpendicular structural trend between salt structures and sub-salt faults in the rift phase, indicate that most salt structures in the study area were triggered halokinetically (Figure 10).

The structural shoulders and margins in the Early Triassic had more uniform and tabular seismic characteristics, consistent with pre-kinematic layers, as compared to the main rift basin of the Dutch-Central Graben.

The transition from a salt pillow (pA) to a passive diapir (dP) in the eastern margin is characterized by layered and onlap seismic reflectors onto the salt diapir's 1 body which transitions into syn-halokinetic sequences (Figure 16). The intra-seismic stratigraphic reflectors of the syn-halokinetic sequences are characterized by seismic reflectors bounded by an upper and a lower local unconformity (Figure 16b). Furthermore, shifting pds around salt diapir 5, where syn-kinematic and syn-halokinetic sediments thickened, elucidate the transition from a salt pillow (pA) to a passive salt diapir (dP) in the rift phase (Figure 17b); this thickening is the evidence that the flanks of the underlying salt structure sank to create the necessary space for salt mobilization and salt flow into the salt diapir. When salt mobilizes into the rising salt diapir, the adjacent convex-downward base of the paleo-depocenter, in the rift stage, flattens out coevally to the change of diapiric growth mode (Figure 17). Additionally, pseudo-downlap stratigraphic reflectors at the pedestal of salt diapir 3 in the northern part of the Dutch-Central Graben were previously seismic paleo-onlap reflectors against the southwestern salt diapir's stem which shifted away from the salt diapir during passive diapirism (Figure 18a-b).

4.12 Tectonic and Kinematic Indicators of Salt Diapirism

The tectono-kinematic indicators of salt diapirism are represented by active faulting in the adjacent seismic stratigraphic sequences, e.g., radial, concentric, and flanking faults. We use the term flanking faults to refer to faults striking parallel to the structural trend of salt walls in map view and not to refer to the faults and fractures emanating away from a rising or evolving salt body, i.e., radial faults. Flanking faults are ubiquitously found across all structural domains of the Dutch-Central Graben. For instance, flanking faults are observed within the stratigraphic sequences encasing salt diapir 7 in the

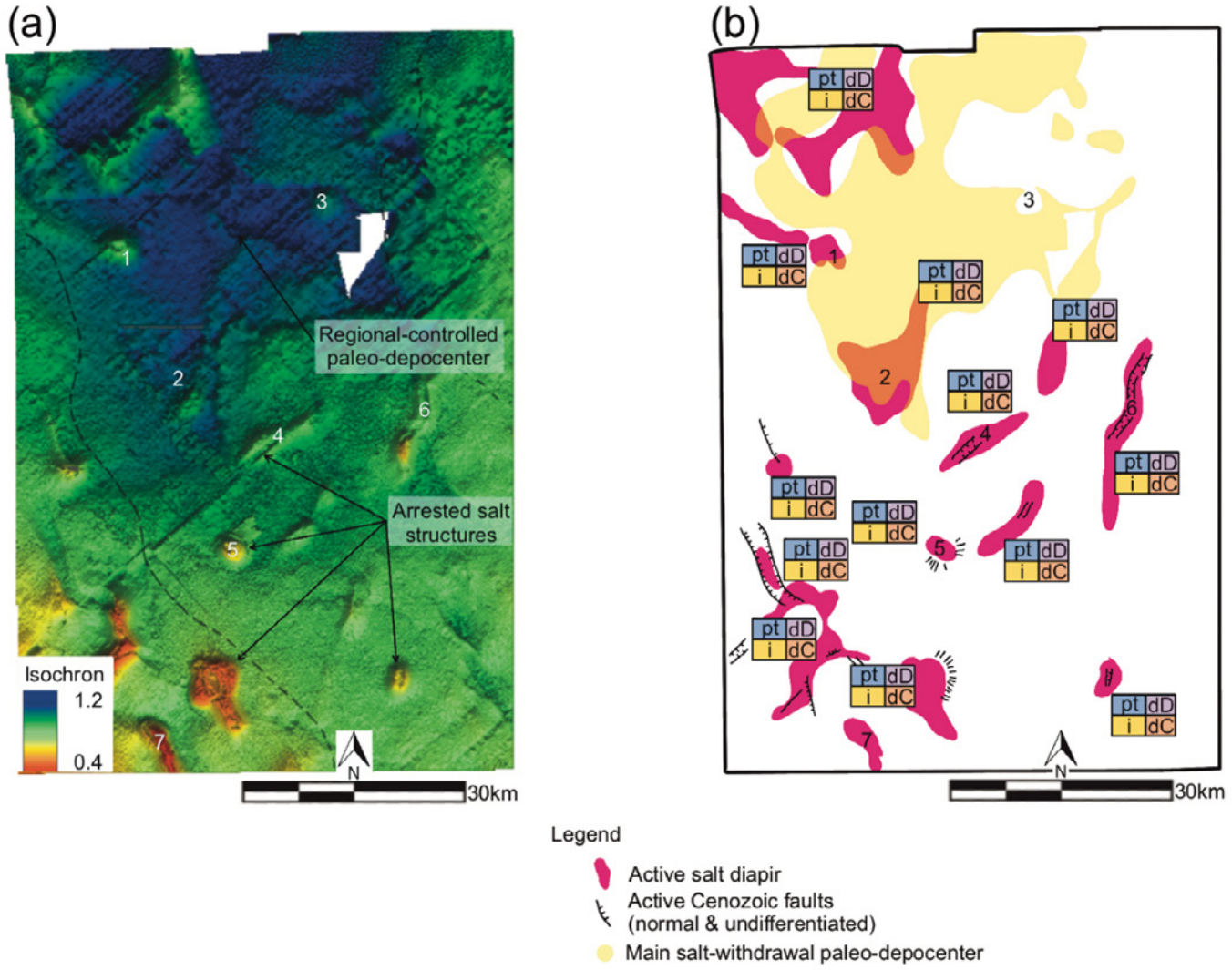

Figure 15 – Qty-Neogene (inversion/contraction and post-inversion) seismic stratigraphic level. **a)** Seabed – Base Neogene (Top Paleogene) TWTT thickness map (isochron). **b)** Synthesis map of the Qty-Neogene mega-stratigraphic sequence in the inversion and post-inversion regional phase showing a main regional-controlled paleo-depocenter, underlying basement faults, and Cenozoic faulting. Salt diapirs 1-7 labeled. Mainly concentric faulting is observed atop elongated salt walls.

western shoulder characteristic of reactive diapirism (Figure 20c).

Radial faults are ubiquitous to all structural domains of the Dutch-Central Graben (Figures 16-20). Similarity attribute maps elucidate that radial faults are easily influenced by the presence of adjacent salt structures (Figure 17c-e). For example, salt diapir 5 in the main rift graben displays complex salt-related radial faults and fault communication along the different structural zones of the salt diapir. Further, radial faults are evident in the rift (Figures 17c and 20c-d) and in the inversion phases (Figures 16-20). Radial faults in the Dutch-Central Graben reach an extent of deformation of c. 5 km in radius (Figure 17e), which transition to polygonal faults, recording the areal extent of the salt diapir's field stress perturbation transitioning into an isotropic field stress. Radial faults in the Dutch-Central Graben are linked to the local stage of passive diapirism of salt diapir 3, which is uncommon (Figure 20c). These radial faults are c. 3-4 km long and are influenced by nearby faults and adjacent salt diapirism.

Radial faults at the salt's roof and carapace in the rift basin are characterized by Y patterns in the arched and uplifted roof within the Paleogene-Neogene seismic stratigraphic sequences in the inversion phase (Figure 16e). Moreover, concentric faults in the northern part of the study area elucidate deformation caused by inversion and the shortening of salt diapirs, which uplifted the salt's diapir roof (Figures 16e-20e).

4.13 Summary

This study analyzed 32 salt structures in the different structural domains of the Dutch-Central Graben, of which 28 are multi-stage salt diapirs. This study identified that salt structures were triggered as, 1) one passive and five reactive diapirs in the west shoulder, 2) two salt anticlines and one reactive diapir in the west margin, 3) ten salt anticlines, two reactive, and one passive diapir in the main rift graben, 4) two salt anticlines, one reactive, and one passive diapir in

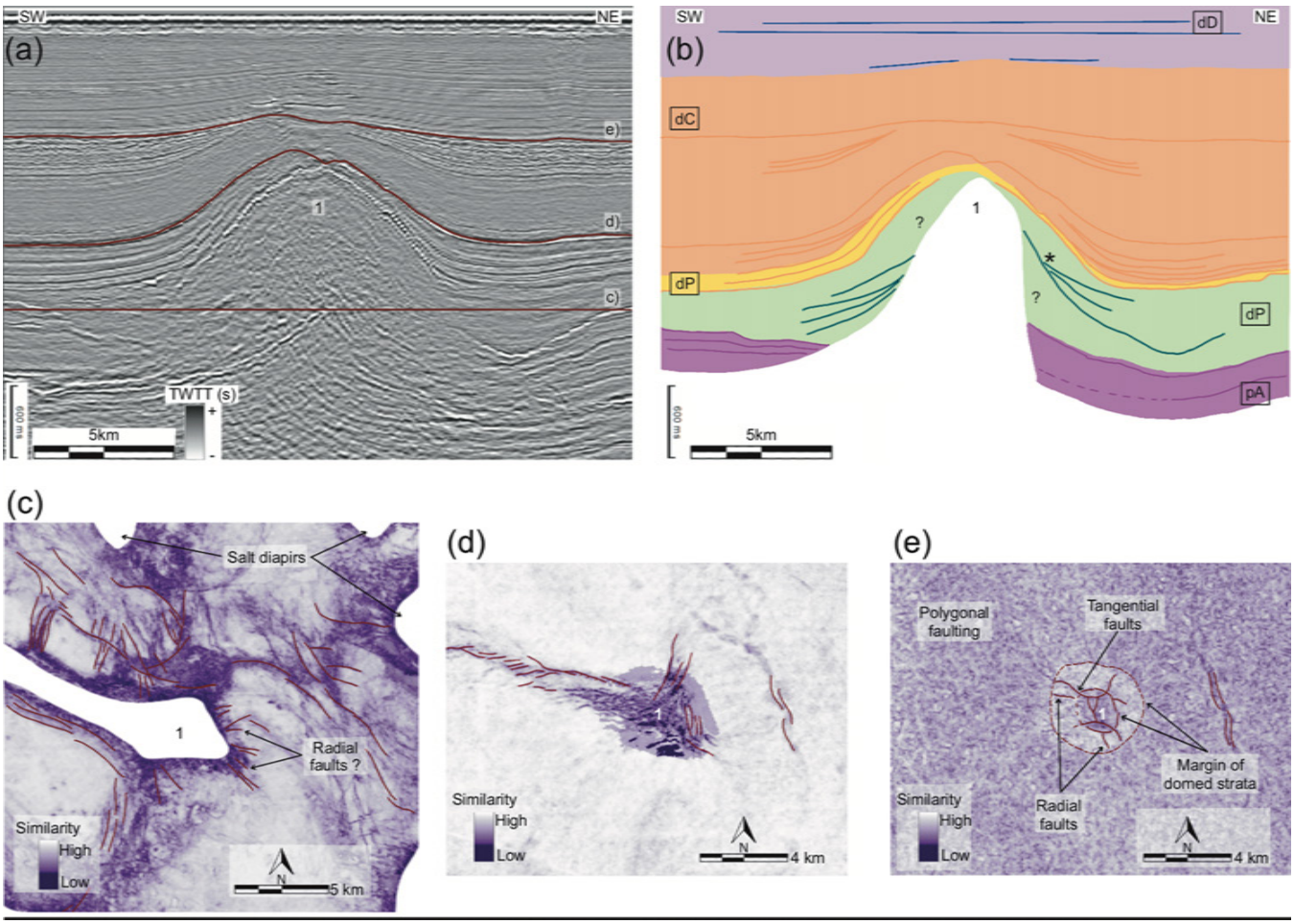

Figure 16 – Multi-stage Salt diapir 1. **a)** Seismic section SW-NE through salt diapir 1 and extracted similarity attribute levels. **b)** Interpreted cartoon of seismic cross-section SW-NE through salt diapir 1 using color codes from local stages after Gaitan and Adam (2023). * in b) represents halokinetic sequences preserved after structural inversion. **c-e)** Similarity volume attribute structure maps. **c)** Extracted at 2.5 ms (TWTT). **d)** Top Cretaceous (Base Cenozoic) horizon. **e)** Top Paleogene (Base Neogene) horizon. Seismic data courtesy of PGS (now TGS). Cross-section reference in Figure 5b.

the eastern margin, 5) and one salt anticline and one reactive diapir in the eastern shoulder.

5 Discussion

This study validated the regional classification for salt structures in *Gaitan and Adam* (2023) in the Dutch-Central Graben, SNS. Additionally, this study showed a deeper evaluation of the different kinematic indicators of halokinetic processes in the Dutch-Central Graben; it highlights that there is a further variability of the controlling mechanisms of salt diapirism in the Dutch-Central Graben and that it is possible discriminate salt structures on a sub-basin scale previously identified and classified in regional studies.

Time-thickness maps derived from the regional seismic mega-stratigraphic sequences formed the first order local framework to chronologically correlate and classify salt diapirs in the Dutch-Central Graben; this is because the complete kinematic evolution of salt diapirs is recorded within the encasing seismic stratigraphic sequences (*Gaitan and Adam*, 2023; *Harding and Huuse*, 2015; *Pichel and Jackson*, 2020).

Generally, the different salt structural trends across the study area evinced diverse drivers and trigger mechanisms for salt diapirism. For instance, salt structural trends trending like the sub-Zechstein salt structural trend were triggered or influenced by tectonic rifting and contraction tectonics. Contrarily, salt structural trends dissimilar to sub-Zechstein salt structural features were controlled by sedimentation and halokinesis. Previous studies identified extensional tectonics and reactive diapirism as the main trigger mechanism for salt diapirism (*Jackson and Hudec*, 2017; *Jackson and Vendeville*, 1994; *Karam and Mitra*, 2016; *Moragas et al.*, 2017; *Vendeville*, 2002; *Vendeville et al.*, 1987; *Vendeville and Jackson*, 1992a). Nevertheless, this study demonstrates that salt diapirs in the main Dutch-Central Graben basin were triggered halokinetically as salt anticlines, whereas reactive diapirism is the main trigger mechanism in the shoulders and margins of the Dutch-Central Graben.

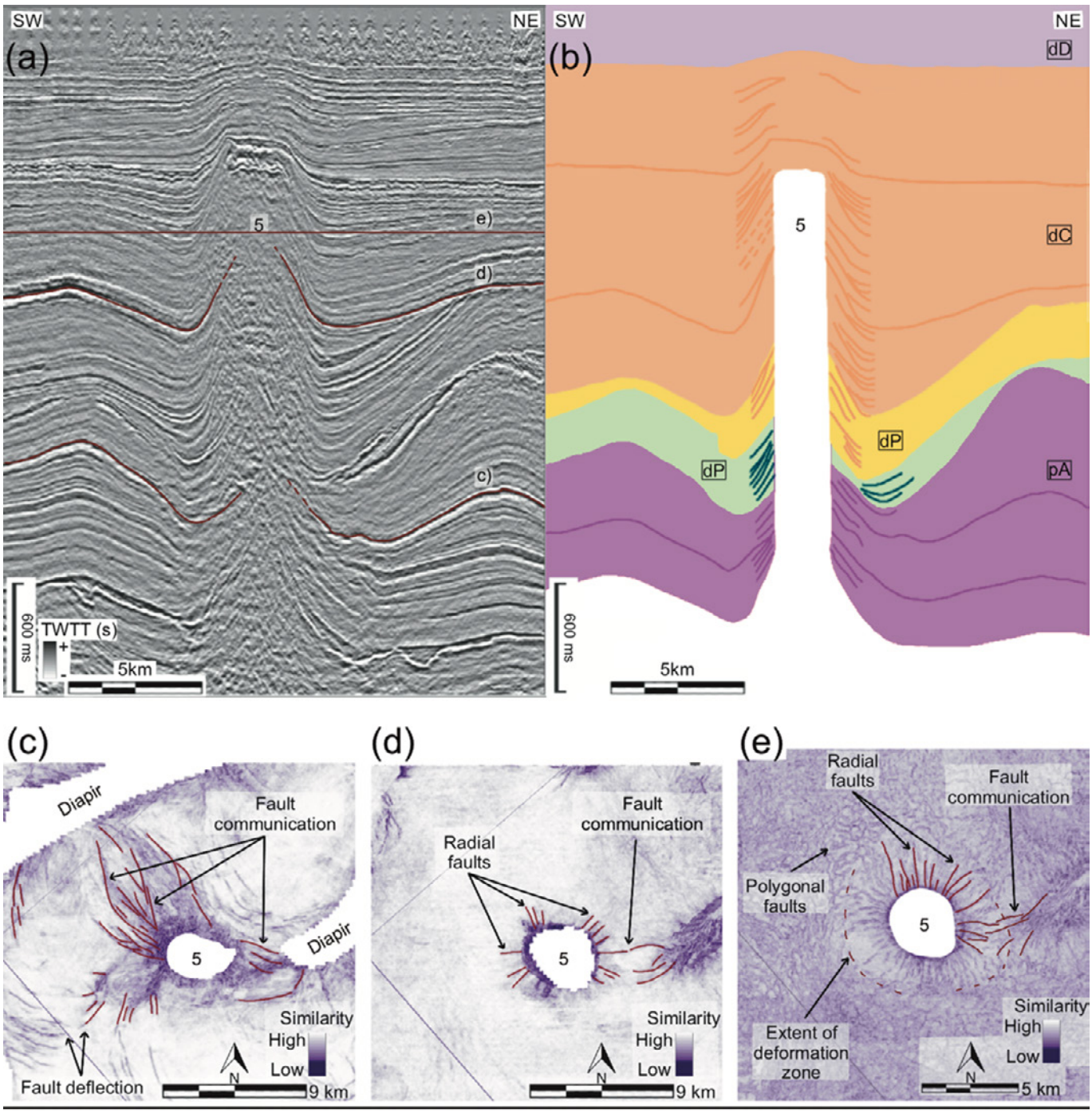

Figure 17 – Multi-stage Salt diapir 5. **a)** Seismic section SW-NE through Salt diapir 5. **b)** Interpreted cartoon of seismic cross-section NW-SE through salt diapir 2 using color codes from local stages after Gaitan and Adam (2023). **c-f)** Similarity volume attribute structure maps. **c)** Top Triassic horizon. **d)** Top Cretaceous (Base Cenozoic) horizon. **e)** Extracted at 1.26 s (TWTT). Seismic data courtesy of PGS (now TGS). Cross-section reference in Figure 5b.

5.1 Controls of Salt Diapirism

5.1.1 Syn-depositional Controls of the Zechstein Salt Layer

As previously discussed in *Gaitan and Adam* (2023) and in agreement with the different syn-sedimentation carbonate-evaporite cycles of the Zechstein Supergroup (*Grant et al.*, 2019; *Peryt et al.*, 2010), the Late Permian Zechstein salt syn-depositional thickness variations controlled the development of salt anticlines as early as in the Early Triassic (*Clark et al.*, 1998; *Stewart*, 2007). This is evidenced by, 1) the NE-SW salt structural trend of salt diapirs in the western shoulder, western margin, and in the main rift basin (Figure 10). Evidently, the NE-SW salt structural trend is perpendicular to the NW-SE sub-salt basement structural fault trend (Figure 9a), 2) the identification of Early Triassic local salt-withdrawal pds across the different structural domains of the Dutch-Central Graben, 3) the early development of now-inverted salt-withdrawal depocenters adjacent to salt diapirs in the main rift basin. Salt halokinetic processes pre-dating the Hardegsen rifting tectonic phase of the North Sea

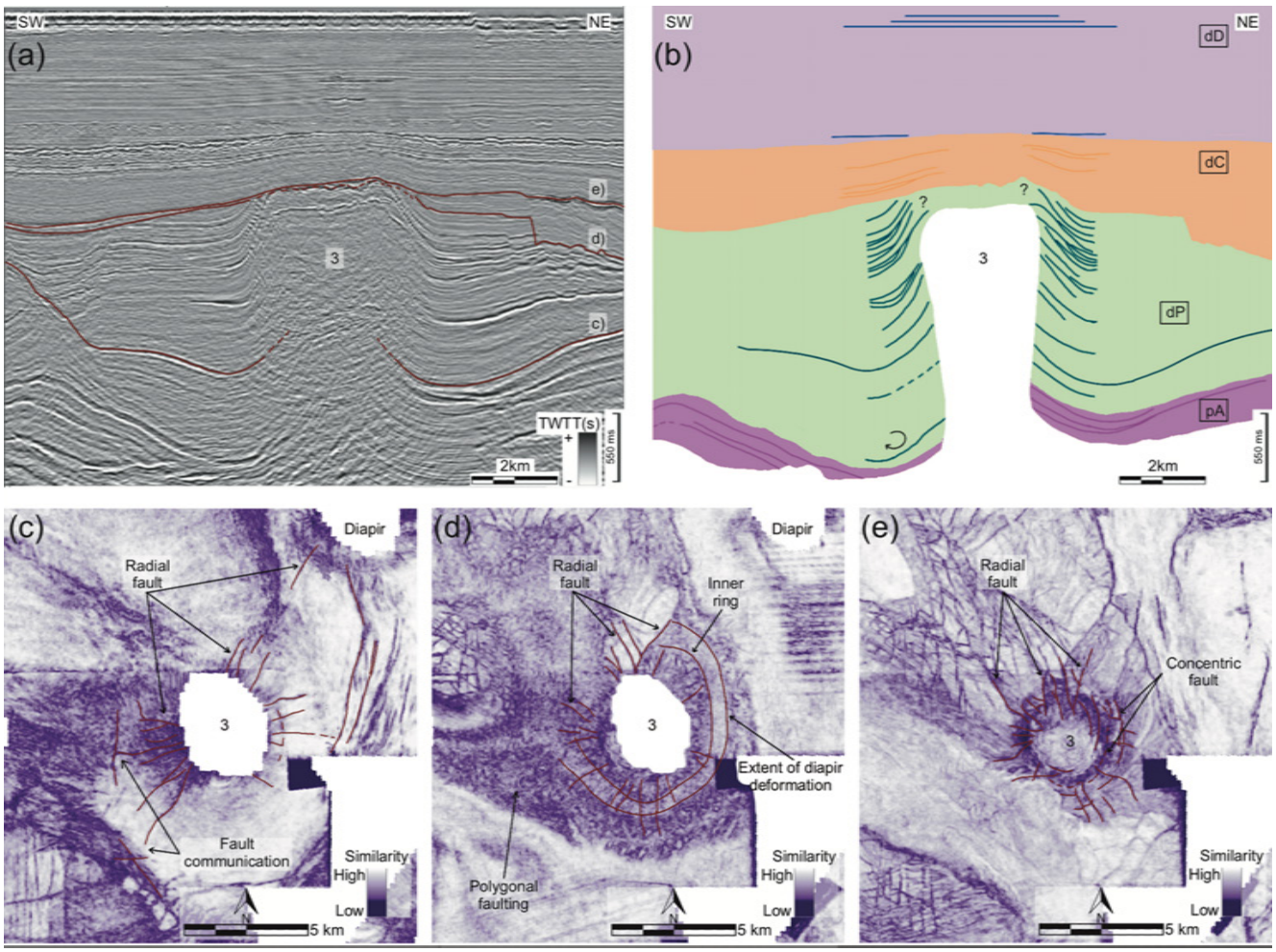

Figure 18 – Multi-stage Salt diapir 3. **a)** Seismic section SW-NE through salt diapir 3 and extracted similarity attribute levels. **b)** Interpreted cartoon of seismic cross-section SW-NE through salt diapir 3 using color codes from local stages after *Gaitan and Adam* (2023). Circular arrow in the southwestern side of salt diapir 3 represents the stratal outward rotation of the pseudo-downlap reflectors. **c-e)** Similarity volume attribute structure maps. **c)** Top Triassic horizon. **d)** Top Jurassic (BCU) horizon. **e)** Top Cretaceous (Base Cenozoic) horizon. Seismic data courtesy of PGS (now TGS). Cross-section reference in Figure 5b.

concurs with the observations discussed in *Harding and Huuse* (2015) documented in the Hantum Fault Zone adjacent to the eastern flank of the Central Graben system.

5.1.2 Basement and Post-salt Syn-depositional Controls

The basement-inherited graben morphology of the Dutch-Central Graben controlled the accumulation and preservation of a thick Mesozoic-Cenozoic cover in the deepest parts of the main rift basin (Figures 10-15). Moreover, rifting tectonics during the Triassic triggered reactive diapirism in the basin marginal areas, e.g., in the shoulders and margins of the Dutch-Central Graben (Figure 10). This agrees to the basement extension and supra-salt development of reactive diapirs demonstrated by physical modeling by *Dooley et al.* (2003) and numerical models in *Hudec and Jackson* (2011).

Mesozoic faults in the Dutch-Central Graben were controlled by active basement-faulting, reactivation of Paleozoic faults, halokinesis, and salt tectonics (Figures 10-13), evidenced by an oblique salt structural trend to the main NNW-SSE trend of sub-salt basement faults. No residual structures were identified that might have controlled the NE-SW structural trend of salt walls in the Dutch-Central Graben, which is congruent with structural analysis of the Dutch-Central Graben by *Preiss and Adam* (2021). Interestingly, tectonic inversion during the Late Cretaceous-Cenozoic occurred along the eastern part of the Dutch-Central Graben, and eastern margin and shoulder and not along the documented sub-salt regional basement faults of the Dutch-Central Graben; evidenced by tectonic uplift and erosion from isochron maps during the Cretaceous (Figure 13b) and Paleogene (Figure 14b).

Regional salt-withdrawal pds shifted from the northwestern part of the Dutch-Central Graben during the Early Triassic (Figure 10b-c) to the southeastern part in the Jurassic during the rift phase (Figure 12b-c). Surprisingly, the seismic stratigraphic sequences in the rift phase in the southern part of the Dutch-Central Graben are thinner than the stratigraphic sequences observed in the northern

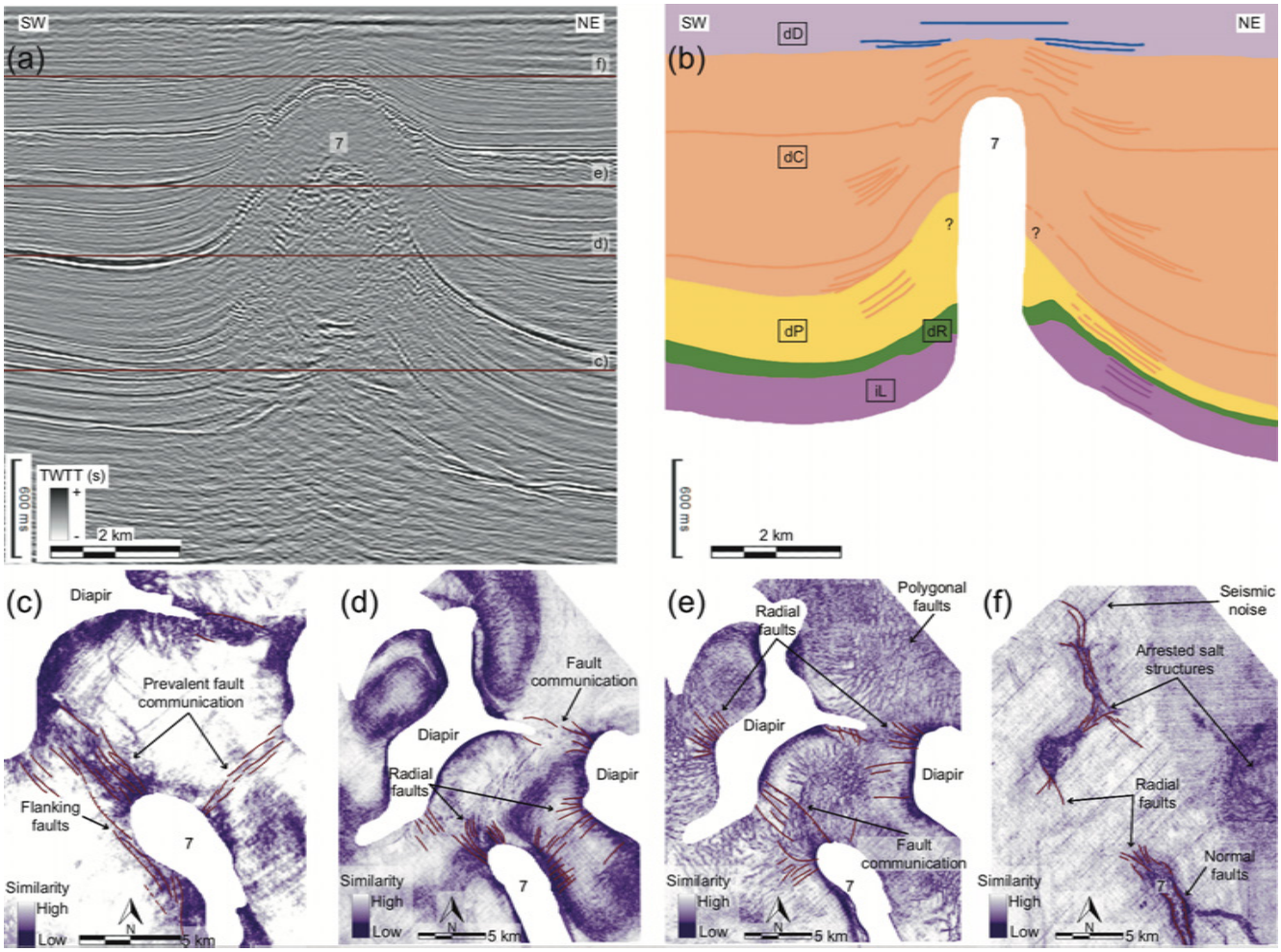

Figure 19 – Multi-stage Salt diapir 7. **a)** Seismic section SW-NE through Salt diapir 7. **b)** Interpreted cartoon of seismic cross-section NW-SE through salt diapir 7 using color codes from local stages after Gaitan and Adam (2023). **c-f)** Similarity volume attribute structure maps. **c)** Extracted at 2.39 ms (TWTT). **d)** Extracted at 1.64 ms (TWTT). **e)** Extracted at 1.18 ms (TWTT). **f)** Extracted at 0.47 ms (TWTT). Seismic data courtesy of PGS (now TGS). Cross-section reference in Figure 5b.

part of the Dutch-Central Graben (Figures 6-7). We speculate that the main controlling factor for this occurrence, aside from local halokinetic processes, was the tectonic evolution of NNE-SSW trending Mesozoic faults. The NNW-SSE sub-salt basement faults had little to no influence in the development and shifting of the salt-withdrawal pds, as Jurassic pds lie atop the sub-salt basement fault in the eastern margin (Figure 12c).

5.2 Chrono-halokinetic Stack Grouping

We grouped salt structures in the Dutch-Central Graben into three different groups to compare the regional variability across the different structural domains and the local variability of salt structures within each structural domain. The different groups were categorized based on their trigger mechanisms shown from the first local stage block at the bottom-right of the chrono-halokinetic stacks (Figure 21). For example, we grouped salt diapirs that were triggered as reactive diapirs (dR) into Group 1, salt diapirs triggered as salt anticlines (pA) into Group 2, and salt diapirs triggered as passive diapirs (dP) into Group 3 (Figure 21).

5.2.1 Group 1

Group 1 represents multi-stage salt diapirs that were triggered in a reactive diapir (dR) stage of salt diapirism. The first chrono-halokinetic stack in Group 1 shows salt diapirs which evolved in a 1-1 regional phase to local stage ratio, e.g., one local stage in the rift phase and one local stage in the inversion phase. Furthermore, a second chrono-halokinetic stack displays a 1-2 regional phase to local stage ratio, i.e., one local stage in the rift phase and two local stages in the inversion phase. The third and last chrono-halokinetic stack also shows a 1-2 regional phase to local stage ratio, i.e., two local stages in the rift and in the inversion phase (Figure 21).

Group 1 contains ten evolving salt diapirs (Figure 22a). Four salt diapirs evolved in three local stages and four salt diapirs in four local stages. The remaining two salt diapirs evolved in five local stages of salt diapirism (Figure 22b). Five reactive diapirs were triggered in the western shoulder, one in the western margin, two in the main Central Graben, and one each in the eastern shoulder and eastern margin.

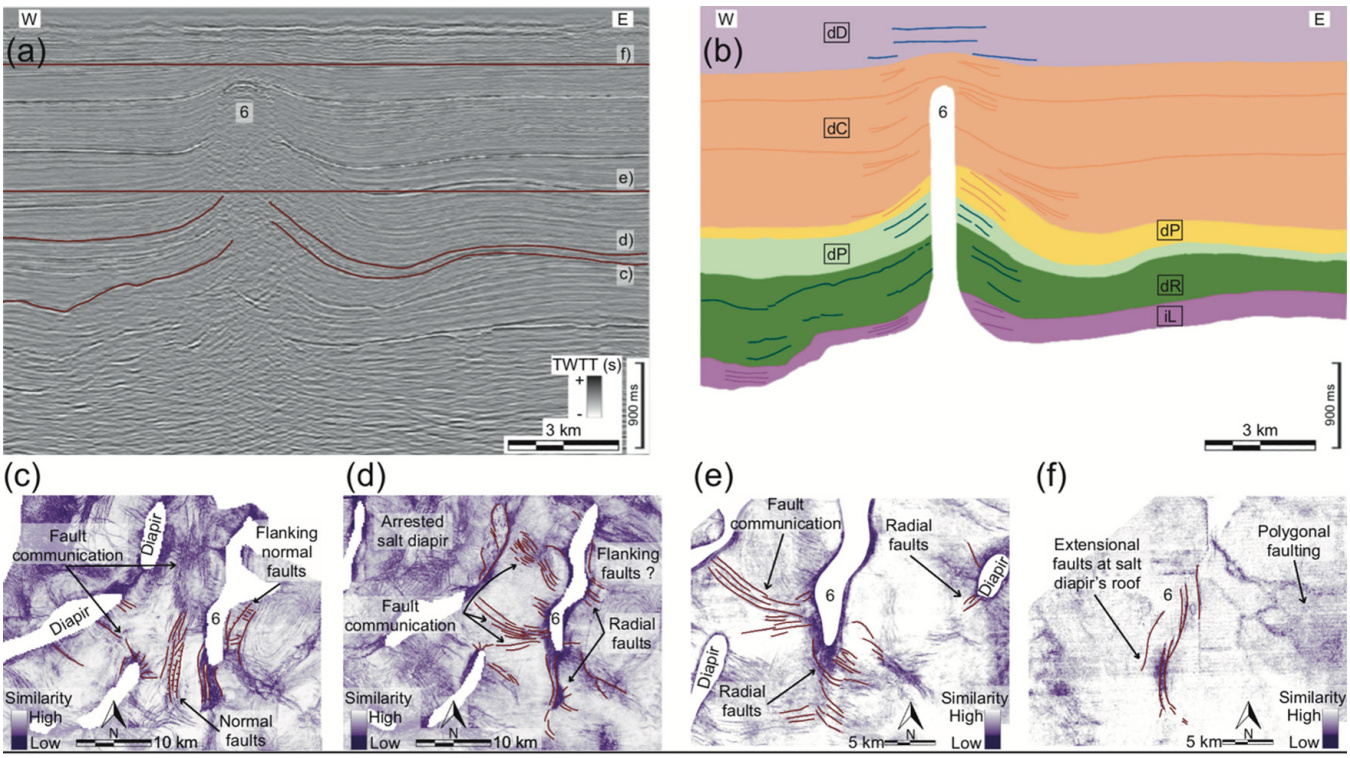

Figure 20 – Salt diapir 6. **a)** Seismic section W-E through Salt diapir 6. **b)** Interpreted cartoon of seismic cross-section W-E through salt diapir 6 using color codes from local stages after Gaitan and Adam (2023). **c-f)** Similarity volume attribute structure maps. **c)** Top Triassic similarity map. **d)** Top Jurassic (BCU). **e)** Extracted at 1.94 s TWTT. **f)** Extracted at 0.60 s TWTT. Seismic data courtesy of PGS (now TGS). Cross-section reference in Figure 5b.

The controlling factors for deformation in Group 1 are, 1) the basin-marginal deformation of the NNW-SSE trending, sub-salt basement faults during the rift phase which triggered NNW-SSE trending reactive diapirism and passive diapirism. Additionally, basin-marginal deformation triggered NNW-SSW trending Triassic faults in the western shoulder and in the northernmost part of the Dutch-Central Graben (Figure 21). The style of basement-involved tectonics was also determined by the original salt thickness of 500-1,000 m (*Maystrenko et al.*, 2013) across the Dutch-Central Graben. Constant thicknesses in the Mesozoic in the western shoulder also implies that the trigger mechanisms were linked to regional tectonics and depositional factors had a minor or negligible influence, 2) the development of NNE-SSW trending Mesozoic faults during extension which triggered NNE-SSW trending reactive diapirs in the western and eastern margins (Wm1, Em1; Figure 21), 3) the thick accumulation of Triassic–Jurassic sediments influenced long-lived passive diapirism (dP) which extended from the rift phase into the inversion phase, 4) and inversion tectonics which squeezed, already stablished, km-tall salt diapirs during the Cenozoic triggering contractional diapirism (dC) (Figure 21).

5.2.2 Group 2

Group 2 represents multi-stage salt diapirs that were triggered in a salt anticline (pA) stage of halokinesis. The first chrono-halokinetic stack in Group 2 shows salt diapirs which evolved in a 1-1 regional phase to local stage ratio, e.g., one local stage in the rift and in the inversion phase. The second chrono-halokinetic stack first displays a 1-2 regional phase to local stage ratio in the rift phase and a 1-1 ratio in the inversion phase. The third and last chrono-halokinetic stack also shows a 1-2 regional phase to local stage ratio, i.e., two local stages in the rift and in the inversion phase (Figure 21). Group 2 contains 15 evolving salt diapirs (Figure 22a). One salt diapir evolved in three local stages, four salt diapirs evolved in four local stages, and ten salt diapirs evolved in five local stages of salt diapirism (Figure 22b). Two salt anticlines were triggered in the western margin, ten in the main Dutch-Central Graben, two in the eastern margin, and one in the eastern shoulder.

The controlling factors for deformation in Group 2 are, 1) an already structured Zechstein Supergroup which controlled the development of local pds during the Early Triassic–Jurassic and triggered salt anticlines in the main rift basin of the Dutch-Central Graben as evidenced by the NNE-SSW salt structural trend of salt structures, e.g., multi-stage salt diapirs CG21-22 and Em22. Moreover, the salt mobilization into the main rift basin and salt flow into salt structures permitted the salt diapiric growth of four-km-tall salt diapirs in the main Dutch-Central Graben, 2) the basin-marginal deformation in the Triassic of the NNW-SSE trending sub-salt basement faults triggered salt anticlines in the western margin (Wm22), 3) the development of NNE-SSW Mesozoic faults which, together with paleo-depocenter formation, triggered NNE-SSW salt anticlines, e.g., Wm21, Em21, and

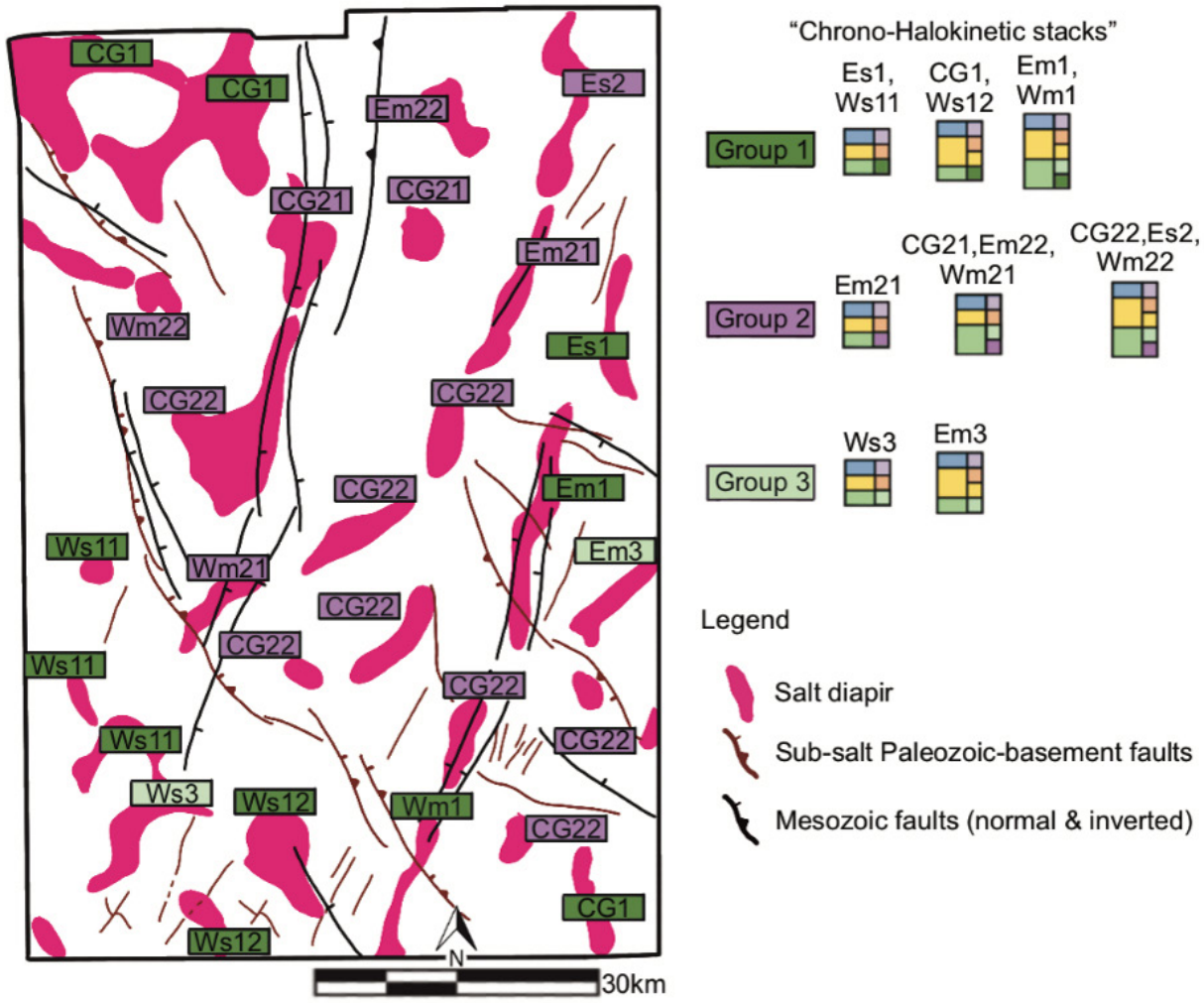

Figure 21 – Synthesis map of salt structures and multi-stage salt diapirs in the Dutch-Central Graben. Map showing regional phases and local stages of salt diapirism using the chrono-halokinetic stacks defined by *Gaitan and Adam* (2023). Em=East margin, Es=East shoulder, CG=Central Graben, Wm=West margin, Ws=West shoulder.

salt diapirs trending NNW-SSW in the northern and southern part of the main rift basin of the Central Graben, 4) the thick accumulation of Triassic–Jurassic sediments influenced long-lived passive diapirism (dP) which extended from the rift phase into the inversion phase, 5) and the inversion tectonics which squeezed, already stablished, km-tall salt diapirs in the Cenozoic triggering contractional diapirism (dC) (Figure 21).

5.2.3 Group 3

Group 3 represents multi-stage salt diapirs that were triggered in a passive diapir (dP) stage of salt diapirism. The first chrono-halokinetic stack in Group 3 shows salt diapirs which evolved in a 1-1 regional phase to local stage ratio, e.g., one local stage in the rift phase and one local stage in the inversion phase. The second and last chrono-halokinetic stack displays a 1-2 regional phase to local stage ratio, i.e., one local stage in the rift phase and two local stages in the inversion phase (Figure 21). Group 3 contains only three evolving multi-stage salt diapirs (Figure 22a). One salt diapir evolved in three local stages and two salt diapirs evolved in four local stages of salt diapirism (Figure 22b). One passive diapir was triggered in the western shoulder, one in the main Dutch-Central Graben, and one in the eastern margin.

The controlling factors for deformation in Group 3 are like in Groups 1 and 2. For example, passive diapirism in the western shoulder was triggered by the destabilization of the salt layer by the NNW-SSE sub-salt basement extension and reactive diapirism (Ws3; Figure 21). Moreover, passive diapirs were also triggered by the interplay between active NNE-SSW trending Mesozoic faults in the southern part of the Dutch-Central Graben. Additionally, sedimentation shifted from the northern part of the study area in the Early Triassic to the southern part of the Dutch-Central Graben from the Early Triassic (Figure 10b-c) to the Jurassic (Figure 12b-c) as evidenced by the location of local pds transitioning from the northern part to the central-southern part of the Dutch-Central Graben. The thick accumulation of Mesozoic sediments directly influenced the long-lived passive diapir stage from the rift phase to the inversion phase (CG3, Em3; Figure 21). Lastly, inversion tectonics triggered contractional diapirism

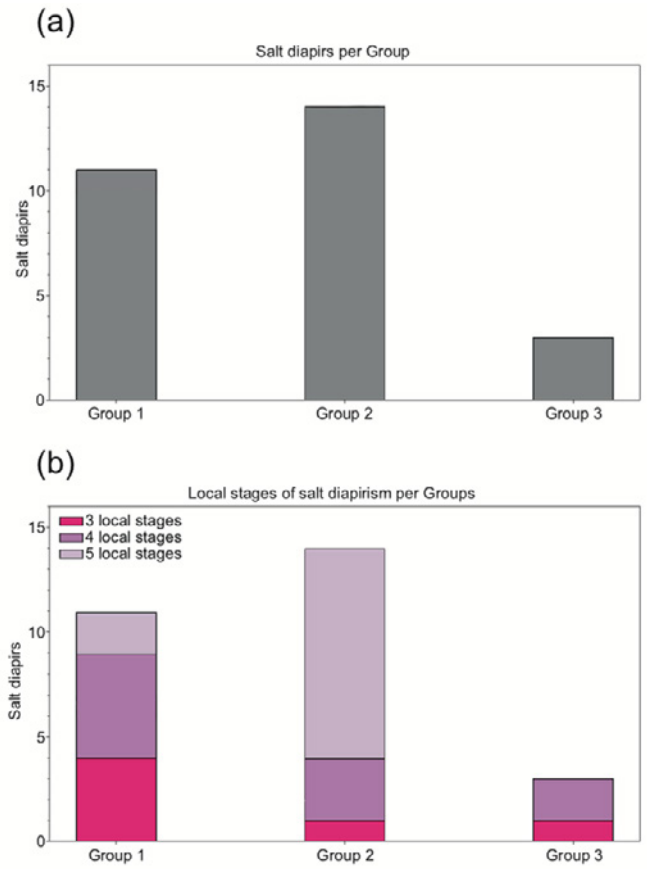

Figure 22 – Summary of salt diapirs in the Dutch-Central Graben per Group. **a)** Number of salt diapirs in each Group. **b)** Number of local stages within the different Groups.

(dC) in the Late Cretaceous–Cenozoic as ubiquitously observed and interpreted across the different structural domains of the Dutch-Central Graben (Figure 21).

5.3 Second Order Salt-related Faulting as Kinematic Indicators for Salt Diapirism

The second order fault structure indicators for salt diapirism are characterized by radial and concentric faults, and fault communication between adjacent salt structures which are found across the different structural domains of the Dutch-Central Graben and along the different structural domains of salt diapirs, e.g., the salt's body and salt's carapace.

Across the different structural domains, fault communication is more common during the salt anticline (pA) stage in the rift phase (Figure 23). Only salt diapir 6 in the eastern margin displayed fault communication with adjacent salt structures during the contractional diapir (dC) stage of salt diapirism (Figure 23f). This observation might imply that fault communication is more likely to develop in salt basins during the rift phase of tectonic deformation.

Radial faulting is common across all the different structural domains of the Dutch-Central Graben and observed along the salt's body and at the salt's carapace. Y-pattern radial faults at the salt's roof were interpreted in the western margin (Figure 21a) and in the main rift graben (Figure 21b). Unsurprisingly, the syn-kinematic and syn-halokinetic seismic stratigraphic sequences evolving during a passive diapir (dP) stage of salt diapirism, are relatively fault free (Figure 21b, f). Interestingly, this study identified syn-halokinetic sequences with clear radial and concentric faults preserved within the seismic stratigraphic sequences in the rift phase (Figure 23a, c, e). We acknowledge that these second order structural features within the rift phase might have been developed during a younger contractional diapir (dC) stage and not necessarily linked to radial and concentric faulting during the rift phase.

Inverted salt-withdrawal local pds are observed only in the main Dutch-Central Graben (Figure 21e). We infer that this was controlled by the high sediment input during the Mesozoic which permitted a long-lived salt structural evolution of salt diapirs which stopped evolving once the supra-salt Mesozoic strata welded against the base of the Zechstein salt horizon. Interestingly, the seismic stratigraphic sequences in the rift phase are the thickest in the northern part of the study area (Figure 23c) and the thickest seismic stratigraphic sequences in the contraction/inversion phase across all structural domains are in the central-southern part of the study area; this latter is evidenced from seismic stratigraphic sequences within the contractional diapir (dC) stage which are the thickest in the western margin (Figure 23a), western shoulder (Figure 23d), and in the eastern margin (Figure 23f).

6 Conclusions

This study successfully applied a sui-generis methodology, utilizing a 3D seismic dataset of the Dutch-Central Graben, for the classification of salt structures and corroborated its applicability in local studies. Additionally, this work builds upon the established methodology by characterizing the local dynamic processes that further controlled halokinesis; it identified that salt diapirs in the Dutch-Central Graben evolved in three to five local stages of salt diapirism during the rift, contraction/inversion, and post-tectonic phases of the SNS. Incorporating fault information into the methodology aided the interpretation of multi-stage salt diapirs. Radial and concentric faulting observed along different salt structural zones provided critical insights into the stages of diapiric growth, salt mobilization, and diapiric collapse. These faults acted as indicators of the dynamic interactions between salt structures and surrounding stratigraphic sequences, offering a more nuanced understanding of the basin's tectonic history. Radial faults did not prove to be characteristic of a particular diapiric stage but were helpful in determining the activity or inactivity of salt structures. The study found a clear dominance of salt anticlines triggered in the Dutch-Central

Figure 23 – Schematic diagrams and correlation of the tectonic-stratigraphic, halokinetic, and kinematic stages of multi-stage salt diapirs 1-3 **(a-c)** and 5-7 **(d-f)** in the study area. **a)** Multi-stage salt diapir 1 in the west margin. **b)** Multi-stage salt diapir 2 in the Central Graben. **c)** Multi-stage salt diapir 3 in the Central Graben. **d)** Multi-stage salt diapir 7 in the west shoulder. **e)** Multi-stage salt diapir 5 in the Central Graben. **f)** Multi-stage salt diapir 6 in the east margin. Em=East margin, CG=main Central Graben basin, Wm=West margin, Ws=West shoulder, Dt=Diapir structural trend (when Dt=N/A, it is a salt stock), Bt=Basement structural trend (nearest/beneath multi-stage salt diapir).

Graben, with about 53% of the studied multi-stage salt diapirs triggered as salt anticlines/pillows, 36% as reactive diapirs, and 11% as passive diapirs. The tallest salt diapirs were triggered during the syn-deposition of the Late Permian Zechstein salt in the main rift graben. The most complex multi-stage salt diapirs evolved through up to five different local stages of salt diapirism. Salt diapirism in the main rift graben was further controlled by rifting in the SNS, which caused the thick accumulation and preservation of Mesozoic sediments, influencing the long-lived passive diapir stage. Salt structures are of increasing societal and economic interest to the energy sector and the energy transition, serving as storage for compressed air, hydrogen, gas, and being relevant for nuclear and water waste management. Thorough evaluation of multi-stage salt diapirs and encasing sedimentary sequences is paramount for understanding the sealing capabilities of salt to mitigate risks and uncertainties. These insights and the classification can be applied locally and in other salt basins around the world.

Acknowledgements

We would like to kindly acknowledge S&P Global for providing the seismic interpretation software Kingdom and TGS (formerly Petroleum GeoServices), for providing the Southern North Sea MegaSurvey 3D seismic dataset.

Author contributions

Both authors contributed to the conceptualization of this project and project administration. Moreover, **Gerardo Gaitan** worked on the investigation, validation, visualization, and writing of this study, whereas **Jürgen Adam** provided supervision and comments.

Data availability

The original dataset, i.e., the MegaSurvey 3D dataset of the Southern North Sea, was kindly provided by Petroleum GeoServices (PGS), now TGS; the dataset was shared under an NDA. The UK sector of the MegaSurvey is now public via the UK National Data Repository (NDR) by the North Sea Transition Authority (NSTA).

Competing interests

The authors declare no competing interests.

Peer review

This publication was peer-reviewed by Mar Moragas and an anonymous reviewer. The full peer-review report can be found here: Review Report.

Copyright notice

References

Cameron, T. D. J., A. Crosby, P. S. Balson, D. H. Jeffrey, G. K. Lott, J. Bulat, and D. J. Harrison (1992), United Kingdom Offshore Regional Report: the Geology of the Southern North Sea, *HMSO for the British Geological Survey, London*.

Clark, J. A., S. A. Stewart, and J. A. Cartwright (1998), Evolution of the NW margin of the North Permian Basin, UK North Sea, *Journal of the Geological Society*, *155*(4), 663–676, doi: 10.1144/gsjgs.155.4.0663.

Coward, M., and S. Stewart (1995), *Salt-influenced structures in the Mesozoic-Tertiary cover of the southern North Sea, U.k*, vol. 65, American Association of Petroleum Geologists, doi: 10.1306/m65604c10.

Davison, I., G. Alsop, N. Evans, and M. Safaricz (2000), Overburden deformation patterns and mechanisms of salt diapir penetration in the Central Graben, North Sea, *Marine and Petroleum Geology*, *17*, 601–618, doi: 10.1016/S0264-8172(00)00011-8.

de Jager, J. (2003), Inverted basins in the Netherlands, similarities and differences, *Netherlands Journal of Geosciences/Geologie en Mijnbouw*, *82*(04), 339–349, doi: 10.1017/s0016774600020175.

de Jager, J., and M. C. Geluk (2007), Petroleum geology, in *Geology of the Netherlands*, edited by T. E. Wong, D. A. J. Batjes, and J. de Jager, p. 241–264, Royal Netherlands Academy of Arts and Sciences.

Dooley, T., K. McClay, and R. Pascoe (2003), 3D analogue models of variable displacement extensional faults: applications to the Revfallet Fault system, offshore mid-Norway, *Geological Society special publication*, *212*, 151–167, doi: 10.1144/GSL.SP.2003.212.01.10.

Doornenbal, H., and A. Stevenson (2010), *Petroleum geological atlas of the Southern Permian Basin area*, EAGE, Houten.

Doornenbal, J. C., H. Kombrink, R. Bouroullec, R. A. F. Dalman, G. De Bruin, C. R. Geel, A. J. P. Houben, B. Jaarsma, J. Juez-Larré, M. Kortekaas, H. F. Mijnlieff, S. Nelskamp, T. C. Pharaoh, J. H. Ten Veen, M. Ter Borgh, K. Van Ojik, R. M. C. H. Verreussel, J. M. Verweij, and G. J. Vis (2019), New insights on subsurface energy resources in the Southern North Sea Basin area, *Geological Society special publication*, *494*(1), 233–268, doi: 10.1144/sp494-2018-178.

Duffy, O., University of Texas at Austin, M. Hudec, F. Peel, G. Apps, A. Bump, L. Moscardelli, T. Dooley, S. Bhattacharya, K. Wisian, and M. Shuster (2023), The role of salt tectonics in the energy transition: An overview and future challenges, *Tektonika*, *1*(1), 18–48, doi: 10.55575/tektonika2023.1.1.11.

Evans, D., N. Petroleumsforening, and Greenland (2003), The millennium atlas : petroleum geology of the central and northern North Sea, *Geological Society of London*, *16*, 389.

Gaitan, G., and J. Adam (2023), Extent and variability of Mesozoic-Cenozoic multi-stage salt diapirs in the Southern Permian Basin, Southern North Sea, *Basin research*, *35*(6), 2078–2117, doi: 10.1111/bre.12791.

Gast, R. E., M. Dusar, C. Breitkreuz, R. Gaupp, J. W. Schneider, L. Stemmerik, M. C. Geluk, M. Geißler, J. Kiersnowski, K. W. Glennie, S. Kabel, and N. S. Jones (2010), Rotliegend, in *Petroleum Geological Atlas of the Southern Permian Basin Area*, edited by J. C. Doornenbal and A. G. Stevenson, pp. 101–121, EAGE Publications b.v., Houten.

Geldart, L. P., and R. E. Sheriff (2004), Seismic Velocity, in *Problems in Exploration Seismology and their Solutions*, chap. 5, pp. 141–180, SEG, doi: 10.1190/1.9781560801733.ch5.

Geluk, M. (2005), Stratigraphy and tectonics of Permo-Triassic basins in the Netherlands and surrounding areas, Ph.D. thesis, Utrecht University, Utrecht, The Netherlands.

Glennie, K. (1998), *Petroleum geology of the North Sea: Basic concepts and recent advances*, 4 ed., Blackwell Science, Philadelphia, PA.

Glennie, K., and D. Provan (1990), Lower Permian Rotliegend reservoir of the Southern North Sea gas province, *Geological Society special publication*, *50*, 399–416, doi: 10.1144/GSL.SP.1990.050.01.25.

Grant, R. J., J. R. Underhill, J. Hernández-Casado, S. M. Barker, and R. J. Jamieson (2019), Upper Permian Zechstein Supergroup carbonate-evaporite platform palaeomorphology in the UK Southern North Sea, *Marine and petroleum geology*, *100*, 484–518, doi: 10.1016/j.marpetgeo.2017.11.029.

Guterch, A., S. Wybraniec, M. Grad, A. Chadwick, C. M. Krawczyk, P. A. Ziegler, H. Thybo, and W. De Vos (2010), Crustal structure and structural framework, in *Petroleum geological atlas of the southern Permian Basin area*, edited by J. C. Doornenbal and A. G. Stevenson, pp. 11–23, EAGE, Houten.

Harding, R., and M. Huuse (2015), Salt on the move: Multi stage evolution of salt diapirs in the Netherlands North Sea, *Marine and petroleum geology*, *61*, 39–55, doi: 10.1016/j.marpetgeo.2014.12.003.

Hodgson, N., J. Farnsworth, and A. Fraser (1992), Salt-related tectonics, sedimentation and hydrocarbon plays in the Central Graben, North Sea, UKCS, *Geological Society special publication*, *67*, 31–63, doi: 10.1144/GSL.SP.1992.067.01.03.

Hudec, M. R., and M. P. A. Jackson (2007), Terra infirma: Understanding salt tectonics, *Earth-science reviews*, *82*(1-2), 1–28, doi: 10.1016/j.earscirev.2007.01.001.

Hudec, M. R., and M. P. A. Jackson (2009), Interaction between spreading salt canopies and their peripheral thrust systems, *Journal of structural geology*, *31*(10), 1114–1129, doi: 10.1016/j.jsg.2009.06.005.

Hudec, M. R., and M. P. A. Jackson (2011), *The salt mine: a digital atlas of salt tectonics: Austin TX, The University of Texas at Austin, Bureau of Economic Geology*, 305 pp., American Association of Petroleum Geologists, Tulsa, OK.

Hudec, M. R., M. P. A. Jackson, and D. D. Schultz-Ela (2009), The paradox of minibasin subsidence into salt: Clues to the evolution of crustal basins, *Geological Society of America bulletin*, *121*(1-2), 201–221.

Jackson, C. A.-L., and S. A. Stewart (2017), Composition, tectonics, and hydrocarbon significance of zechstein supergroup salt on the United Kingdom and Norwegian continental shelves, in *Permo-Triassic Salt Provinces of Europe, North Africa and the Atlantic Margins*, pp. 175–201, Elsevier, doi: 10.1016/b978-0-12-809417-4.00009-4.

Jackson, M. P. A., and M. R. Hudec (2017), *Salt tectonics: Principles and practice*, Cambridge University Press, Cambridge, England, doi: 10.1017/9781139003988.

Jackson, M. P. A., and B. C. Vendeville (1994), Regional extension as a geologic trigger for diapirism, *GSA Bulletin*, *106*(1), 57–73, doi: 10.1130/0016-7606(1994)106<0057:REAAGT>2.3.CO;2.

Jackson, M. P. A., B. C. Vendeville, and D. D. Schultz-Ela (1994), Structural dynamics of salt systems, *Annual review of earth and planetary sciences*, *22*(1), 93–117, doi: 10.1146/annurev.ea.22.050194.000521.

Karam, P., and S. Mitra (2016), Experimental studies of the controls of the geometry and evolution of salt diapirs, *Marine and petroleum geology*, *77*, 1309–1322, doi: 10.1016/j.marpetgeo.2016.05.010.

Maystrenko, Y. P., U. Bayer, and M. Scheck-Wenderoth (2012), Regional-scale structural role of Permian salt within the Central European Basin System, *Geological Society special publication*, *363*(1), 409–430, doi: 10.1144/sp363.19.

Maystrenko, Y. P., U. Bayer, and M. Scheck-Wenderoth (2013), Salt as a 3D element in structural modeling — Example from the Central European Basin System, *Tectonophysics*, *591*, 62–82, doi: 10.1016/j.tecto.2012.06.030.

Moragas, M., J. Vergés, T. Nalpas, E. Saura, J. D. Martín-Martín, G. Messager, and D. W. Hunt (2017), The impact of syn- and post-extension prograding sedimentation on the development of salt-related rift basins and their inversion: Clues from analogue modelling, *Marine and petroleum geology*, *88*, 985–1003, doi: 10.1016/j.marpetgeo.2017.10.001.

Nikolinakou, M. A., P. B. Flemings, and M. R. Hudec (2014), Modeling stress evolution around a rising salt diapir, *Marine and petroleum geology*, *51*, 230–238, doi: 10.1016/j.marpetgeo.2013.11.021.

Peryt, T. M., M. C. Geluk, A. Mathiesen, J. Paul, and K. Smith (2010), Zechstein, *Petroleum geological atlas of the Southern Permian Basin area*, pp. 123–147.

Pharaoh, T. C., M. Dusar, M. Geluk, F. Kockel, C. M. Krawczyk, P. Krzywiec, M. Scheck-Wenderoth, H. Thybo, O. Vejbaek, and J.-D. Van Wees (2010), Tectonic evolution, in *Petroleum geological atlas of the Southern Permian Basin area*, edited by J. C. Doornenbal and A. G. Stevenson, pp. 25–57, EAGE, Houten.

Pichel, L. M., and C. A.-L. Jackson (2020), Four-dimensional variability of composite halokinetic sequences, *Basin research*, *32*(6), 1277–1299, doi: 10.1111/bre.12428.

Preiss, A. D., and J. Adam (2021), Basement fault trends in the Southern North Sea Basin, *Journal of structural geology*, *153*(104449), 104,449, doi: 10.1016/j.jsg.2021.104449.

Quirk, D. (1993), Interpreting the upper carboniferous of the Dutch Cleaver Bank High, in *Petroleum Geology of Northwest Europe: Proceedings of the 4th Conference*, vol. 4, edited by J. R. Parker, pp. 697–706, The Geological Society, London, doi: 10.1144/0040697.

Remmelts, G. (1995), Fault-related salt tectonics in the southern North Sea, the Netherlands, *AAPG Special*

Volumes, *65*, 261–272.

Remmelts, G. (1996), Salt tectonics in the southern North Sea, the Netherlands, in *Geology of Gas and Oil under the Netherlands*, edited by H. E. Rondeel, D. A. J. Batjes, and W. H. Nieuwenhuijs, pp. 143–158, Springer Netherlands, Dordrecht, doi: 10.1007/978-94-009-0121-6_13.

Schnabel, M., V. Noack, N. Ahlrichs, and C. Hübscher (2021), A comprehensive model of seismic velocities for the Bay of Mecklenburg (Baltic Sea) at the North German Basin margin: implications for basin development, *Geo-marine letters*, *41*(2), doi: 10.1007/s00367-021-00692-w.

Sears, R. A., A. R. Harbury, A. J. G. Protoy, and D. J. Stewart (1993), Structural styles from the Central Graben in the UK and Norway, *Geological Society London Petroleum Geology Conference series*, *4*(1), 1231–1243, doi: 10.1144/0041231.

Stewart, S. (2007), Salt tectonics in the North Sea Basin: a structural style template for seismic interpreters, *Geological Society special publication*, *272*, 361–396, doi: 10.1144/GSL.SP.2007.272.01.19.

Stewart, S., and M. Coward (1995), Synthesis of salt tectonics in the southern North Sea, UK, *Marine and Petroleum Geology*, *12*(5), 457–475, doi: 10.1016/0264-8172(95)91502-G.

Stewart, S. A. (2006), Implications of passive salt diapir kinematics for reservoir segmentation by radial and concentric faults, *Marine and petroleum geology*, *23*(8), 843–853, doi: 10.1016/j.marpetgeo.2006.04.001.

Veen, J., S. V. Gessel, and M. D. Dulk (2012), Thin- and thick-skinned salt tectonics in the Netherlands: a quantitative approach, *Geologie En Mijnbouw*, *91*(4), 447–464, doi: 10.1017/S0016774600000330.

Vejbæk, O. V., C. Andersen, M. Dusar, G. F. W. Herngreen, H. Krabbe, K. Leszczyński, G. K. Lott, J. Mutterlose, and A. S. Van der Molen (2010), Cretaceous, *Petroleum geological atlas of the southern Permian Basin Area*, pp. 195–209.

Vendeville, B. (2002), A new interpretation of Trusheim's classic model of salt-diapir growth, *Gulf Coast Association of Geological Societies Transactions*, *52*, 943–952.

Vendeville, B., and M. Jackson (1992a), The fall of diapirs during thin-skinned extension, *Marine and Petroleum Geology*, *9*(4), 331–354, doi: 10.1016/0264-8172(92)90047-I.

Vendeville, B., P. Cobbold, P. Davy, P. Choukroune, and J. Brun (1987), Physical models of extensional tectonics at various scales, *Geological Society special publication*, *28*, 107–195, doi: 10.1144/GSL.SP.1987.028.01.08.

Vendeville, B. C., and M. P. A. Jackson (1990), Physical modeling of the growth of extensional and contractional salt tongues on continental slopes (abs.), *AAPG bulletin*, *74*(5), 784.

Vendeville, B. C., and M. P. A. Jackson (1992b), The rise of diapirs during thin-skinned extension, *Marine and petroleum geology*, *9*(4), 331–354.

Ziegler, P. A. (1990), *Geological Atlas of Western and Central Europe*, Shell Internationale Petroleum Maatschappij B.V., Geological Society Publishing House (Bath).